Mechanism of Hydrogen Spillover on Metal-Doped Carbon Materials: Surface Carboxylic Groups Are Key

Javier Navarro-Ruiz, Jérémy Audevard, Mathieu Vidal, Cristian Campos, Iker del Rosal, Philippe Serp, Iann Gerber

Mechanism of Hydrogen Spillover on Metal-Doped Carbon Materials: Surface Carboxylic Groups are Key

Javier Navarro-Ruiz,[a] Jérémy Audevard,[b] Mathieu Vidal,[b] Cristian H. Campos,[c] Iker Del Rosal,[b] Philippe Serp,[b,] Iann C. Gerber[a,*]*

[a] *LPCNO, INSA−CNRS−UPS, Université de Toulouse, 135 Avenue de Rangueil, 31077 Toulouse, France*

[b] *LCC−CNRS, Université de Toulouse, UPR 8241 CNRS, INPT, Toulouse, France*

[c] *Departamento de Físico-Química, Facultad de Ciencias Químicas, Universidad de Concepción, Edmundo Larenas 129, Casilla 160-C, Concepción, Chile*

Abstract. Hydrogen spillover (H-spillover) is the surface migration of activated hydrogen atoms from a metallic particle, on which they are generated, onto a support. The phenomenon has been widely studied because of its implication in hydrogen storage and in catalytic reactions involving hydrogen. Its existence on carbon materials is well established, but questions remain regarding its mechanism and the involvement of surface oxygen groups. In this study, we combined experimental work with chemical modeling to study the mechanisms of H-spillover on a representative system including a carbon material presenting basal and prismatic surfaces: oxidized carbon nanotubes doped with Pd. The experimental results, supported by those of modeling, show that the surface carboxylic acid groups are the key species allowing the spillover of hydrogen on carbon materials to take place. The carboxylic groups can also work in combination with phenol groups to facilitate H-spillover. If the concentration of these groups is too low, the H-spillover does not operate, except in the case of the addition of water, which serves as a shuttle for the protons. This study leads to a deeper understanding of the long-debated issue of H-spillover on carbon materials, and provides insight into designing systems with enhanced properties.

Keywords: Hydrogen spillover, palladium, carbon materials, DFT calculations, oxygen functional groups, surface chemistry

Table of Contents artwork

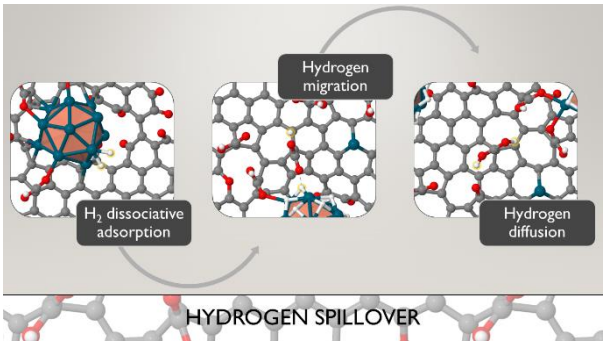

1. INTRODUCTION

Spillover is defined as the transport of a species, adsorbed or formed on a specific surface (or site), to another surface, which, under the same conditions, does not adsorb or form this species.[1] More specifically, Boudart *et al*. called "spillover" the migration of H atoms from metallic particles to a support they can invade.[2] Since the first experiments carried out sixty years ago,[3] a growing body of indisputable evidence exists for the occurrence of hydrogen spillover (H-spillover) in a wide range of systems. Typical applications of the H-spillover effect include hydrogen storage and catalytic hydrogenations,[4] as well as hydrogen production from water splitting.[5] A H-spillover mechanism should consist of several steps. In the first one, molecular hydrogen is activated and dissociated on a transition-metal (TM) particle in close contact with the support. Secondly, the migration of H species from the metal particles to the support should occur. This step is highly dependent on the nature of metal and support (reducible *vs* non-reducible oxides, carbon materials).[1, 6-8] The last two steps consist in the surface diffusion, which can be assisted by water,[9-10] and recombination of H species on the support surface. The nature of the H-species, in the form of H^+, $H^\bullet$, both H^+ and $H^\bullet$ or H^-, depending on the nature of the support, has been discussed for a long time in the literature.[11]

On carbon materials, the H-spillover mechanism has been explored because of its relevance for hydrogen storage, and to a lesser extent for its implication in catalytic reactions.[8, 12-13] The first step in H-spillover on TM particles is to dissociate H_2. Although several metals or semi-metals have been investigated, Pd and Pt are the most studied since the first experiments of Robell and Boudart.[14] The dissociative chemisorption of H_2 on these metals is facile,[15-16] and accompanied by the formation of strong metal-hydrogen (M-H) bonds,[17] the binding energies of which are coverage dependent.[18] This is a very unfavorable starting point for H-spillover from a metal surface to the surface of a defect-free carbon material.[19-20] Indeed, high-energy barriers (46-62 $kcal.mol^{-1}$) have been systematically predicted for migration of one H atom from a fully saturated Pt cluster to such a carbon surface.[17, 19-20] Experimental and theoretical results converge towards the fact that the majority of physisorbed $H^\bullet$ on a defect-free carbon is expected to associatively desorb as H_2.[8] Spilt-over hydrogen can thus be seen as an unstable electron donor located at the carbon surface, which needs to be stabilized by a surface receptor site. It has been proposed that spilt-over hydrogen could be reversibly stored on the carbon material as adsorbed H^+ and as electrons in the bulk,[21] as proposed for H-spillover on reducible oxides, where H atoms migrate as neutral H^+-e^- pairs *via* sequential proton-coupled electron transfer.[7, 22] On carbon, both species (H^+ and e^-) migrate onto the support surface by means of

protonic and electronic conduction, which must be exhibited by the support.[23] The spilt-over hydrogen could be stabilized by oxygen-containing functional groups (OFGs) present on most carbon materials,[8] as proposed for H-spillover on non-reducible oxides, where H-spillover is assisted by oxygenated molecules,[7, 24] or others gaseous molecular shuttles.[25] Stabilization by reactive defects resulting from carbon vacancies has also been proposed,[8, 26] but such a mechanism should not be the dominant one considering the low concentrations of such species and the high stability of the C-H bonds formed.[27-28]

Different factors have been identified as affecting the H-spillover on carbon materials. First, the presence of OFGs enhanced surface diffusion, or reversible adsorption of the spilt-over H atoms, even if surface functionalization of the support can decrease its specific surface area and pore volume.[23, 29-34] This results from an improved migration from the metal to the support, but also from a higher dispersion of the metallic phase on functionalized supports.[23, 32-33, 35] In the presence of epoxy groups in the vicinity of a Pt cluster, the migration of one H atom is easy, with an energy barrier of 9.2 kcal.mol^{-1} per H atom.[17] Similar results were reported for Ni clusters.[36] Based on deuterium TPD experiments, Guerrero-Ruiz *et al*. have proposed that carboxylic and/or lactonic groups should be involved in H-spillover, whereas phenolic and carbonyl groups seem to be less efficient for the migration of D atoms and/or for their collection.[30] The superiority of semiquinone groups as receptors for the spilt-over hydrogen was proposed by Yang *et al*.[33] This latter work reported a strong (and irreversible) binding of the spilt-over hydrogen with the lactone groups forming a carboxylic group and a C-H bond. NMR and Raman studies have evidenced that small amounts of carboxylic groups contribute to improved spillover efficiency.[37] A synergistic role of water and surface oxygen groups has also been reported.[31] Beside the concentration and type or surface oxygen species, the specific surface area of the support,[38] and the metal particle dispersion[39] and composition[40] have been shown to play a role in the spillover.

From this literature analysis, it seems obvious that "imperfections" of the carbon material, such as OFGs and defects, play a crucial role in the H-spillover mechanism. These imperfections affect the bonding of the particle on the support, the binding energy of the hydrogen molecules or atoms on the metal, the migration energy of the H atoms from the metal to the support and, finally, the diffusion of hydrogen on the carbon material. The exact role of these imperfections, and in particular of OFGs, definitively needs further studies, as it may be at the origin of the often observed discrepancies between theoretical and experimental studies, but also between different experimental studies.[41] The nature of the H-species involved in H-

spillover (radicals, protons, hydrides, activated hydrogen) is still unclear, and further work is needed to gain further information on that issue. Here, experience and modeling using density functional theory (DFT) calculations are combined to study H-spillover mechanisms on a representative carbon material system: Pd-doped oxidized carbon nanotubes (CNTs).

2. MATERIALS AND METHODS

2.1 Experimental details

CNT supports. Carbon nanotubes were produced by catalytic CVD in a fluidized bed reactor using ethylene as the carbon source.[42] The produced CNTs were purified (dissolution of the catalyst) with an aqueous solution of H_2SO_4 (50 vol%) under reflux for 4 h. Finally, the CNTs were oxidized by treatment with HNO_3.[42] The final product was collected and dried at 80 °C overnight. Finally, the oxidized CNTs were treated or not at 400, 600, 800 and 1000 °C under pure argon for one hour to yield CNT_{400}, CNT_{600}, CNT_{800} and CNT_{1000}.

Pd/CNT catalyst preparation. A dry impregnation method was used to prepare the palladium catalysts supported on the different CNTs. The desired amount of palladium(II) nitrate solution [$Pd(NO_3)_2 \cdot 2H_2O$] was added to acetone (10 mL) containing 1 g of CNTs[42] to yield 1.2 wt% Pd on CNTs. The solution was sonicated at room temperature for 1 hour and magnetically stirred overnight. The solution was then filtered and washed with acetone. The resulting solid was dried in an oven at 120 °C overnight. Finally, the catalyst was reduced in a horizontal tube furnace under a flow of argon and hydrogen (20 vol% H_2) at 300 °C for 2 h (10 °C min^{-1}).

Characterization. The elemental analyzes were carried out on a Perkin Elmer 2400 series II elemental analyzer. The Pd content in the Pd/CNT catalysts was measured by inductively coupled plasma optical emission spectroscopy (ICP-OES) with a Thermo Scientific ICAP 6300 instrument.

The samples were analyzed by X-ray photoelectron spectroscopy at using a VG Escalab MKII spectrophotometer, which operated with a non-monochromatized Mg Kα source (1253.6 eV). Laboratory NAP-XPS measurements were done with an EnviroESCA (SPECS GmbH, Berlin, Germany).[43-44] The focused, monochromatic Al Kα X-ray source (1468.7eV, 42W, 14kV) is separated from the measurement chamber by a silicon nitride window, and the hemispherical energy analyzer is under ultra-high vacuum ($<1 \times 10^{-8}$ mbar) due to a three-stage differential pumping system between the analysis section and analyzer. The analyzer entrance aperture (nozzle) has a diameter of 300 μm and the usual working distance is 1–2 times the nozzle

diameter. Samples were pressed into individual wells of a stainless-steel sample holder and measured first as received under vacuum conditions (p~1 10^{-6} mbar). After that a gas mixture of H_2/N_2 (5/95) was introduced into the analysis region using a mass flow controller. Then the samples were measured in this atmosphere at a pressure of 1 mbar. Survey spectra were acquired with a pass energy of 100eV, a step size of 1.0 eV and a dwell time of 0.2 seconds. Pd 3d, O1s, and C1s core level spectra were acquired with a pass energy of 50eV, a step size of 0.1 eV and a dwell time of 0.2 seconds. The residual energy shift of the binding energy scale after environmental charge compensation by the gas was corrected for all spectra with respect to the emission line of aliphatic carbon at 285 eV.

High-resolution microscopy analyzes were performed using a JEOL JEM 2100F equipped with a field emission gun (FEG) operating at 200 kV with a spot resolution of 2.3 Å and a JEOL JEM-ARM200F Cold FEG operating at 200 kV with a point resolution of >1.9 Å. The particle size distribution was determined by manual measurement of enlarged micrographs of different areas of the TEM grid (at least 300 particles). The Pd_{SA}/Pd_{NP} ratio (a numerical ratio) was measured from STEM-HAADF analyses of at least 500 elements. The reported size distribution in atomic percentage of Pd (based on total number of atoms) in each size range was obtained by calculating the number of atoms (N) in each Pd particle assuming a spherical shape using an equation described in the literature.[45] The dispersion of Pd was calculated from a universal mathematical relationship between the average relative size of metal crystallites and their dispersion.[46]

The specific surface area and pore volume were determined from N_2 adsorption/desorption isotherms at – 196 °C using a Micromeritics instrument. Before analysis, all samples were degassed under vacuum at 120 °C for 6 h. The calculation of the DFT, basal plane, and "non-basal plane" surfaces and the respective ratios has been performed as described in the literature.[47-48] The Raman spectra were obtained on a micro-Raman assembly (Una labram HR800 Jobin Yvon spectrometer). A laser of 532 nm wavelength was used as the excitation source with a maximum power of 7 mW. Powder X-ray diffraction (XRD) patterns were obtained at room temperature with a PANalytical X'PERT PRO diffractometer, using Cu K_α radiation (λ = 1.54187 Å) and a parabolic MPD mirror for Cu radiation.

Temperature-programmed desorption (TPD) measurements were carried out using the 3Flex (Micromeritics) combined with a mass spectrometer (Cirrus 2, MKS Spectra Product). The samples (approximately 50 mg) were pretreated under He (50 mL/min) at 120 °C (10 °C/min) for 1 h to clean their surface. The sample was reduced at 150 °C for 2 h at 5 °C/min under a

flow of 5% H_2/Ar. The solid was then purged with helium at 50 °C until the TCD baseline remained stable before commencing temperature programmed desorption at a ramp of 10°C/min up to 1000 °C. The released products were analyzed by mass spectroscopy. The following fragments (m/z) were recorded: 2, 15, 18, 28, and 44 corresponding to hydrogen (H_2), methane (CH_4), water (H_2O), carbon monoxide (CO) and carbon dioxide (CO_2), respectively.

2.2 Computational details

Periodic DFT calculations were performed using the *ab initio* plane-wave pseudopotential approach as implemented in the Vienna Ab initio Simulation Package (VASP 5.4).[49-50] The Perdew−Burke−Ernzerhof[51] exchange−correlation functional within the generalized gradient approximation was chosen and van der Waals interactions were taken into account through the D3 method of Grimme[52] with zero-damping function. The innermost electrons were replaced by a projector-augmented wave (PAW) approach,[53-54] while the valence monoelectronic states were expanded in a plane-wave basis set with a cut-off energy of 450 eV. As previously computationally modeled and described,[55] the supported metal catalyst consists of an O-functionalized graphene (including experimentally probed abundant OFGs and point defects) as carbon support, together with a single Pd atom embedded in a single vacancy and an adsorbed Pd_{13} cluster, the latter being hydrogenated with a ratio between adsorbed hydrides and surface metal atoms above unity. All the systems considered for the present study are neutral, and Γ-centered 3×3×1 *k*-point[56] grid was employed as a good compromise between accuracy and computational cost. Spurious interactions between the modelled slab and its perpendicular periodic images were eliminated by adding a vacuum region by at least 10 Å, and by considering a dipole correction to the total energy along the *z*-direction.[57] Iterative relaxation of atomic positions proceeded until the change in total energy was less than 10^{-6} eV and the residual forces on any direction were less than 0.015 eV $Å^{-1}$. Transition states were first located by the Climbing Image version of the Nudged Elastic Band, CI–NEB method,[58-59] and then properly optimized using the Quasi–Newton algorithm. Finally, they were proven to show a single imaginary frequency by diagonalizing the numerical Hessian matrix, in which each atom is displaced with a step of 0.015 Å in both positive and negative directions of each coordinate. All computed energies are presented as potential energies; thus, entropies are not considered. Thermal and vibrational contribution from several steps was verified to typically modulate the relative energy positions (reactant/transition state/product) by less than 2 kcal·mol^{-1}, and thus has not been applied to all cases.

3 RESULTS AND DISCUSSION

3.1 Experimental study on H-spillover on Pd-doped carbon nanotubes

3.1.1 Characterization of the carbon nanotube support

The CNTs were produced, purified and oxidized according to procedures already described.[42] Since H-spillover can be influenced by the physicochemical properties of the support, the textural, structural and surface chemistry properties of the CNTs were investigated (**Table S1**). **Figure S1** shows representative SEM, TEM and HRTEM micrographs of the CNTs. The CNT powder (220 m^2 g^{-1}) is composed of agglomerates of size 5-100 μm, and the mean external diameter of CNTs is 13 nm. The nitric acid treatment creates some damage on the tube walls (**Figure S1c**). DFT calculations derived from N_2 adsorption data were used for the determination of basal plane, prismatic and defect surfaces of CNTs.[48] The percentages of prismatic (edges), basal, and defect (surface steps or surface functional groups) surfaces of CNTs are: 58, 31 and 11 (**Figure S1d**). The I_D/I_G ratio of around 1 (from Raman analyses) points to a significant concentration of structural defects on this support. The crystallite size (L_c from XRD) and the typical inter-defect distance (L_D from Raman[60]) are also characteristic of a graphitic material presenting defects. The d_{002} value corresponds to a graphitization degree[61] of 38%. The surface chemistry was probed by TPD and XPS analyses. In XPS, the presence of defects and functional groups in carbon materials introduce new peaks and alter the linewidth and peak position of the C *1s* peak. The full width at half-maximum (FWHM) of the C 1s peak has been used to assess the graphitic nature of carbon, with a larger FWHM corresponding to a more disordered structure.[62] The obtained values (0.72 eV) indicates a moderate graphitization degree of CNTs.[42] The best fit for the main C *1s* spectrum was obtained by deconvoluting the profile into seven line shapes (3 C-C peaks, 3 C-O peaks and a π- π * shake-up peak, **Figure S2**),[63] and their respective parameters and attributions are given in **Table S2**. The C/O at. ratio was 16.5, pointing to a high concentration of oxygen due to the nitric acid oxidative treatment. This result can be rationalized by a high proportion of defects on the pristine CNTs and by their high surface area ($S_{prismatic}$ + S_{defect} = 42 %, **Figure S1d**). The quantification of OFGs presented in **Table S2** shows that the CNTs contains high amount of all of them. TPD-MS analysis allows characterizing OFGs of carbon materials,[64] which decompose, releasing CO and/or CO_2 at different temperatures. The CO_2 and CO spectra of CNTs are shown on **Figure S3**, and the quantification of these groups is given in **Table S3**. The CNT support contains carboxylic groups of various strength (CO_2 at 200/300 °C),[65] carboxylic anhydride (CO_2 and CO at ~450 °C),[66] lactone (CO_2 ≈ 580 °C),[66-68] phenol (CO at ~ 720 °C),[66, 68] ether and semiquinone (CO at

~ 820 °C),[66, 68-70] and quinone/pyrone/chromene (CO at T ~ 880 °C)[67-69] surface groups. Considering the specific surface area of CNTs and the fact that the hexagonal unit cell of graphene contains two carbon atoms having an area of 0.052 nm^2, so 38.5 C nm^{-2}, it was possible to calculate the density of OFGs (**Table S4**). These data were used to model by means of periodic DFT simulations an O-functionalized carbon support,[55] which was used for the modeling study (section 3.2).

3.1.2 Characterization of the Pd-doped CNTs

Pd-doped CNTs (Pd/CNT) with a nominal Pd loading of 1.2 wt % were prepared by wet impregnation from Pd nitrate. From ICP analyses, the Pd loading was 1.09 % wt%. The specific surface area of this sample was 232 m^2 g^{-1}. This sample shows a homogeneous distribution of Pd nanoparticles (Pd_{NP}), as shown on **Figure 1a**.

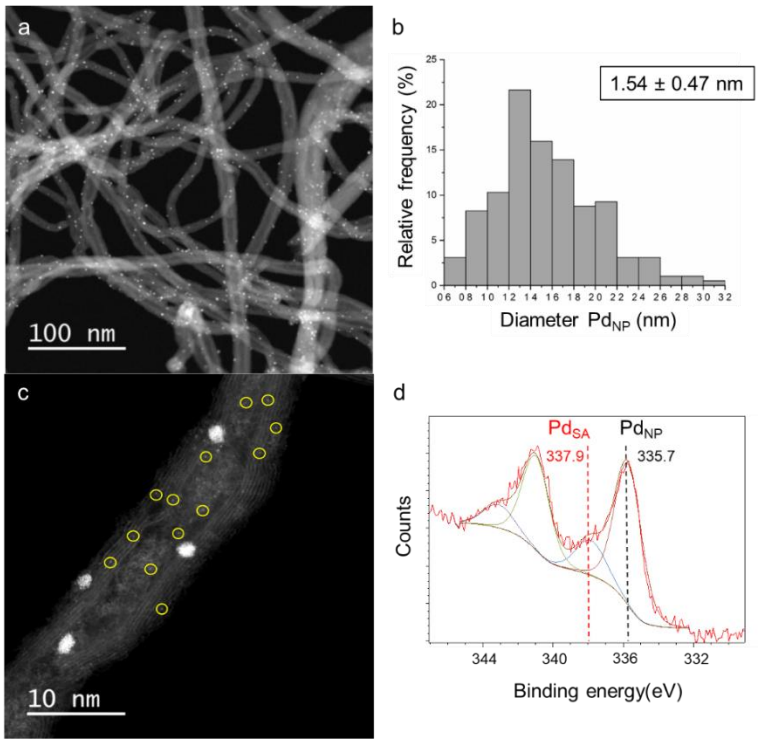

Figure 1. (a) STEM-HAADF micrographs of the Pd/CNT sample. (b) Particle size distributions (from STEM-HAADF micrographs) for Pd/CNT based on total particle number. (c) STEM-HAADF micrographs of Pd/CNT. (d) XPS Pd 3d high-resolution spectra of Pd/CNT.

The measured mean Pd_{NP} size was 1.5 nm (**Figure 1b**). Particle size distributions based on total number of Pd atoms is given on **Figure S4**. The small Pd_{NP} size obtained on CNTs should be related to a high amount of OFGs well distributed on the CNT surface that can act as nucleation centres for Pd_{NP}.[29, 37, 71] The coexistence of Pd single atoms (Pd_{SA}) and Pd_{NP} on this sample is visible on **Figure 1c**. These two species coexist in commonly used commercial carbon-

supported TM catalysts.[72] The ratio Pd_{SA}/Pd_{NP} (a number ratio) was determined to be of 3 for this sample from STEM-HAADF analyses. The sample was also characterized by XRD, XPS, and TPD/MS analysis. In XRD, due to the relatively low metal loading and high metal dispersion, the diffraction peak associated with Pd(111) was of too low intensity to be exploited. XPS analysis was performed on the catalyst to probe the Pd oxidation state and charge transfer (**Figure 1d**). The deconvoluted XPS spectrum for Pd 3d exhibits two pairs of doublets, assigned to $Pd^{(0)}$ and $Pd^{\delta+}$ species. The binding energy of the metallic feature (Pd_{NP}) is ≈ 0.6 eV higher than that of Pd bulk (335.1 eV), which may arise from the small size of Pd_{NP} and/or charge transfer with the support.[73] The $Pd^{\delta+}$ species should be related to small Pd clusters and particularly Pd_{SA} that experienced significant charge transfer with the support.[74]

3.1.3 Experimental studies of H-spillover on Pd/CNT

It is known that the spilt-over H species readily reacts under mild conditions with tungsten oxide WO_3 (yellow powder) to form dark blue H_xWO_3.[75] Hydrogen molecules accomplish the reduction only above 200 °C.[76] As shown in the photographs of **Figure S5**, the WO_3 alone exhibited an unchanged color after H_2 treatment for 10 min. at 20 °C. When mixed with minute amounts of Pd/CNT, a dark blue color is observed after 3 min., demonstrating that H_2 dissociation and extended H-spillover occurred on Pd/CNT. It is inferred that the significant H-spillover should be attributed to the high concentration of OFGs on the carbon support.[29] Indeed, it was recently shown that a higher OFG concentration on carbon supports (per surface unit) allows a more extended H-spillover.[77] The surface chemistry of the Pd/CNT was probed by TPD experiments (**Figure S6**). The CO_2 TPD profiles of the support and of the reduced Pd/CNT sample (**Figure S6a**) show that a significant amount of carboxylic groups act as anchoring sites for Pd_{NP}.[78] Indeed, the narrow peak at 190 °C is characteristic of a catalytic decomposition of surface groups, and should be associated to the decomposition of the –COOPd interface in the catalyst (surface acetato ligands).[79] This interface may have been formed either during sample preparation or after its reduction and further air exposure. As H-spillover is operative on this catalyst, it can also occur during catalyst reduction at 300 °C. This could explain the decrease of carboxylic anhydrides and phenol/carbonyl groups on Pd/CNT compared to CNTs (**Figure S6b**). Indeed, H-spillover arising from TM particles facilitates the reduction of some OFGs on carbon materials at relatively low temperatures.[13, 80] Compared with H_2-molecule-involving reduction, H-spillover can reduce the contents of OFGs of porous carbon more effectively.[80] For the H_2 desorption profiles (**Figure S6c**), the peak starting at high temperature present on the bare support grows significantly for the Pd catalyst. This peak was

attributed to stable C-H functionalities, which should be generated thanks to H-spillover on Pd_{NP} during the catalyst reduction step.[81] Few amounts of H_2 are also released in the 200-600 °C temperature range. Water is also released in the same temperature range (**Figure S6d**). One possible explanation to this could be that some groups are formed thanks to H-spillover during the reduction of the catalyst, which can decompose during TPD by producing either H_2 or preferably H_2O. Froudakis et al.'s simulation have shown that desorption of spilt-over hydrogen bound to surface OH groups occurs more favorably as water rather than molecular hydrogen.[17]

To follow the H-spillover, a particular experiment was performed in the TPD apparatus. First, the reduced Pd/CNT sample was purged with helium at 120 °C for 1 h to clean its surface. The sample was then re-reduced at 150 °C for 2 h at 5 °C min^{-1} under 5% H_2/N_2 flow. Since H-spillover already occurs at room temperature on Pd/CNT (**Figure S5**), extended H-spillover is expected under these conditions.[77] Then, the flow of H_2 was switched to helium and the sample was cooled to 50 °C. TPD-MS was finally performed to quantify the amounts of H_2, H_2O, CO, and CO_2 released. **Figure 2** shows the results obtained as well as those performed on the reduced Pd/CNT, which have been exposed to the air.

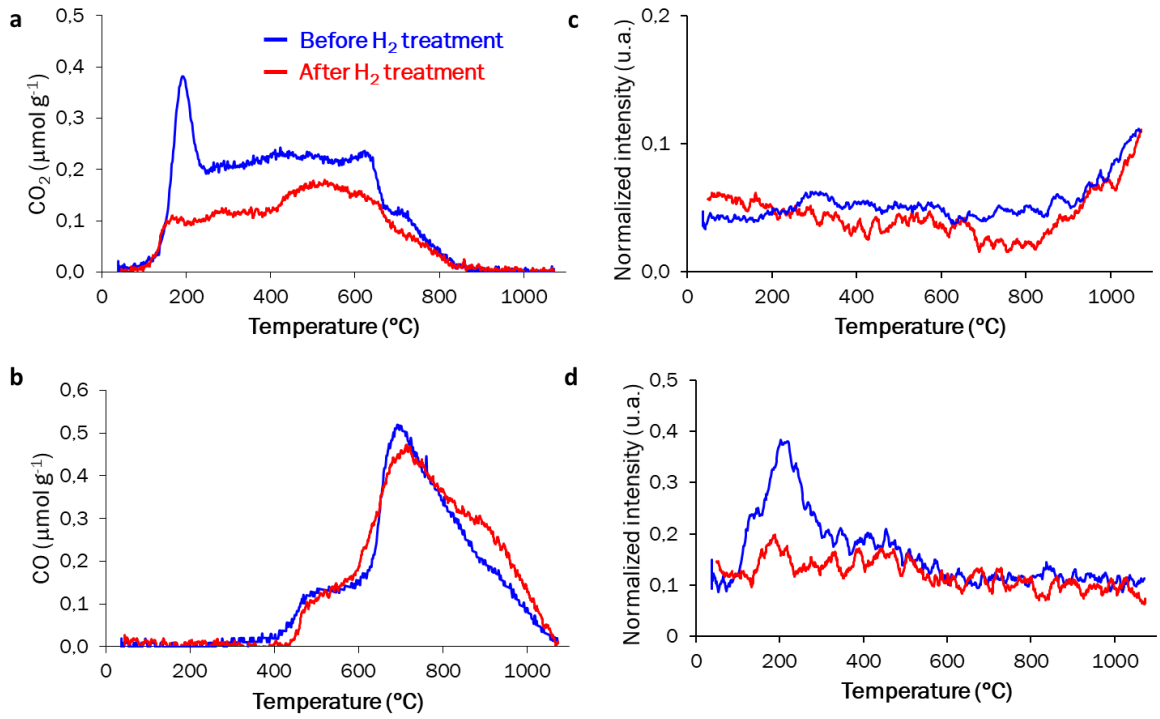

Figure 2. (a) CO_2 TPD profiles of the Pd/CNT before and after H_2 treatment. (b) CO TPD profiles of the Pd/CNT before and after H_2 treatment. (c) H_2 TPD profiles of the Pd/CNT before and after H_2 treatment. (d) H_2O TPD profiles of the Pd/CNT before and after H_2 treatment.

The CO_2-releasing groups concentration decreases due to H-spillover (**Figure 2a**). As far as CO-releasing groups are concerned (**Figure 2b**), the one that decomposed at medium temperatures are slightly decreasing while the more stable species are slightly increasing. The creation of basic carbon surface, generally attributed to very stable quinone/pyrone/chromene,[82] thanks to H-spillover has already been reported.[83] As the–COOPd interface disappears after the H_2 treatment at 150 °C, it is reasonable to propose that it should be formed upon air exposure.[79] For supported Pd catalysts, H_2 desorption from Pd species (either absorbed or chemisorbed H_2) has been reported to occur at relatively low temperatures; and typically, below 50 °C.[84] Consequently, these desorption peaks are not visible on **Figure 2c**. The amount of stable C–H functionalities, does not change significantly between the two experiments. A significant decrease of H_2O desorption is noticed after the H_2 treatment (**Figure 2d**).

From these experiments on Pd/CNT, it is clear that H-spillover operates and that it contributes to a modification of the surface chemistry. Globally, the concentration of CO_2-releasing OFGs decreases significantly and to a lower extent the one of some CO-releasing OFGs (phenol, ether, carbonyl). On the other hand, the concentration of very stable groups (quinone/pyrone/chromene and C–H functionalities) is slightly increasing. Some of us recently report that such phenomena can contribute to catalyst deactivation during hydrogenation reactions.[77]

3.1.4 Influence of oxygen-containing functional groups on H-spillover on Pd/CNT

To probe the possible influence of the type and concentration of OFGs on the extent of H-spillover, four different Pd-doped CNT samples were prepared from Pd nitrate on CNTs presenting various amounts of OFGs. To modulate the concentration of OFGs, the oxidized CNTs were heat-treated at 400 (CNT_{400}), 600 (CNT_{600}), 800 (CNT_{800}) and 1000 °C (CNT_{1000}). The influence of heat treatment at 400 °C on the TPD profiles is shown on **Figure S7**. This treatment eliminates the carboxylic groups and part of the anhydride groups, while lactones are not significantly affected. The slight decrease of phenol groups during the heat treatment at 400 °C could be related to possible rearrangements, such as the reaction of two neighboring hydroxyl groups forming ether bridges between rings.[85] XPS analyses were conducted to probe the surface chemistry of the four heat-treated supports. For the O 1s region, a model based on four main components was used as presented in **Table S5**.[63-64, 67] Peak *I* (530.5-530.6 eV) is associated to carbonyl oxygen in quinone groups. The peak *II* (531.8-531.9 eV) corresponds to

C=O groups in ketones, aldehydes or carboxyl; this peak has sometimes been associated also to the presence of oxygen atoms in hydroxyl groups.[67] The peak *III* (533.1-533.2 eV) has been attributed to phenol and non-carbonyl (ether-type) oxygen atoms in esters and anhydrides.[86] The peak *IV* (534.3) corresponds to -OH in carboxylic groups and has also been attributed to epoxides.[87] XPS and TPD analyses on CNTs oxidized by HNO_3 have shown that this acid treatment not only introduced carboxyl, carbonyl, and phenol surface groups, but also generated ether-type oxygen groups between the graphitic layers.[88] As expected, compared to CNT_{400}, the amount of oxygen decreases in the samples heated at 600, 800 and 1000 °C. Nevertheless, it should be noted that the amount of oxygen in CNT_{1000} is higher than in CNT_{600} and CNT_{800}. This may be due to the reaction of active defects, created during the heat treatment at 1000 °C, with water vapor, O_2, and/or CO_2 from the atmosphere upon exposure to ambient conditions after the annealing procedure.[89] Indeed, heat treatment of carbon materials at high temperatures induces the decomposition of surface groups and reconstruction of the carbon surface, creating reactive defects such as vacancies, Stone-Wales defects or loops.[90] Type *IV* group (carboxylic groups) is particularly affected by the annealing, and the remaining groups should be the more stable ones (quinones, semiquinones and ether groups[88]). In the case of CNT_{1000}, the groups which are formed upon air exposure are mainly of type *II* and *III*.

Table 1 shows the characterization of the Pd-doped CNT series. ICP analyses show that the Pd loading decreases as the temperature of the CNT heat-treatment increases, from 1.1 for Pd/CNT_{400} to 0.7 for Pd/CNT_{1000}.

Table 1. Characterization of the Pd-doped CNT series.

Catalyst	Pd (%)	Pd_{NP} (nm)	D (%)	Pd_{SA}/Pd_{NP}	%spillover
Pd/CNT	1.1	1.5	67.0	3	100
Pd/CNT_{400}	1.1	2.5	44.5	5	79.9
Pd/CNT_{600}	1.1	3.5	33.8	6	70.3
Pd/CNT_{800}	0.9	5.3	24.0	4	33.1
Pd/CNT_{1000}	0.7	4.9	25.7	3	0

This can be related to a decrease of the concentration of OFGs that act as nucleation center for Pd deposition during the impregnation procedure. **Figure S8** shows representative low-resolution STEM micrographs of the four samples. Some large Pd_{NP} are visible at low

magnifications for samples Pd/CNT_{600}, Pd/CNT_{800} and Pd/CNT_{1000}. **Figure S9** shows representative high-resolution STEM-HAADF micrographs of the four samples; palladium single atoms are visible on all samples. Particle size distributions (from STEM-HAADF micrographs) are shown in **Figure S10**. The Pd_{NP} size increases from 1.5 nm for Pd/CNT to 5.3 nm for Pd/CNT_{800}. This can be a consequence of a better diffusion of Pd atoms on the defunctionalized supports. The mean Pd_{NP} size of the Pd/CNT_{1000} sample is slightly smaller than the one of Pd/CNT_{800}. The Pd_{SA}/Pd_{NP} ratio is not significantly affected by the annealing. This could be the result of the creation of stabilizing sites for Pd_{SA} during the heat treatment, such as carbon vacancies.[91] The samples were characterized by XPS to evaluate the C/O ratio, the type of OFGs and the metal state. For the O 1s region (**Figure 3** and **Table S6)**, the same model based on four main components is used as in **Table S5**.

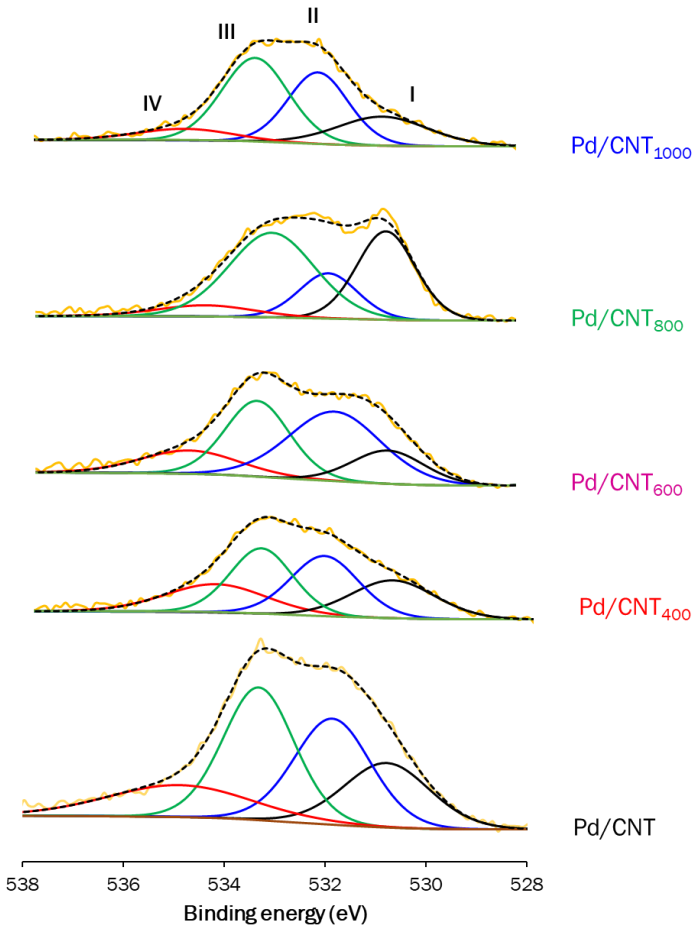

Figure 3. XPS O 1s high resolution spectra of the carbon-supported palladium catalysts.

First, it is notable that surface re-oxidation occurred during sample preparation, since Pd/CNT_{600}, Pd/CNT_{800} and Pd/CNT_{1000} all present a higher concentration of oxygen compared to the bare supports. Such a phenomenon has already been reported when carbon-supported catalysts are prepared from nitrate salts.[92] Indeed, during catalyst calcination under an inert atmosphere (denitrification), water vapor and various nitrogen oxides (NO, NO_2, N_2O_4, and N_2O_5) are produced. Thus, OFGs can be created by (catalyzed) oxidation with nitrogen oxides. Samples Pd/CNT_{800} and Pd/CNT_{1000} present the lower percentage of carboxylic groups (*Type IV* < 0.4 at. %), identified as important for H-spillover.[30, 37] In addition, sample Pd/CNT_{1000} is still the sample that presents the lower concentration of OFGs. The deconvoluted XPS spectra for Pd 3d (**Table S7**) exhibit two pairs of doublets, assigned to $Pd^{(0)}$ (335.4-335.7 eV) and $Pd^{\delta+}$ and species (337.1-337.6 eV). The binding energies of the metallic feature is slightly lower than that of the Pd/CNT sample (335.7 eV), which may arise from the larger Pd particle size in this series. The higher contribution of the $Pd^{(0)}$ component in samples Pd/CNT_{800} and Pd/CNT_{1000} can be tentatively attributed to the presence of larger Pd_{NP} in these two samples. All samples present $Pd^{(0)}$, necessary for H-spillover.

The H-spillover was experimentally probed for all the Pd-doped CNT series using the WO_3 reduction test performed at 20 °C for 5 min (**Figure S11a**). To quantify the obtained results, UV-Vis Diffuse Reflectance Spectroscopy (UV-Vis DRS) analyses were performed on the resulting powders (**Figure S11b**). The values obtained from spectroscopy were normalized by given 100 % to the highest value obtained with Pd/CNT, and 0 % for the Pd/CNT_{1000} (**Figure S12**, black bars and **Table 1**). These data were normalized by the total amount of Pd (**Figure S12**, red bars) and by the total amount of Pd present on the surface of Pd_{NP} (**Figure S12**, blue bars). The general tendency observed is a decrease of H-spillover for the samples treated at high temperatures. This decrease starts to be significant on Pd/CNT_{800} and a complete absence of H-spillover is observed on Pd/CNT_{1000}. No linear correlation could be drawn between the atomic surface concentration of the OFGs of type *I-III* determined by XPS (**Table S6**) and the extent of H-spillover (**Figure S13**). The only type of OFGs that shows a clear tendency is group *IV*, with an increase of H-spillover associated to an increase in carboxylic groups (**Figure 4**). The evolution of H-spillover normalized by surface Pd atoms (**Figure S12**, blue bars) is difficult to rationalize since particle size could affect the heat of adsorption of H_2 (that increases significantly below 3 nm[93]), the formation of a β-hydride phase[94] or the H-coverage[95] on the Pd surface. However, even considering this normalization, a decrease of H-spillover is noticed on sample Pd/CNT_{800} compared to Pd/CNT_{600}.

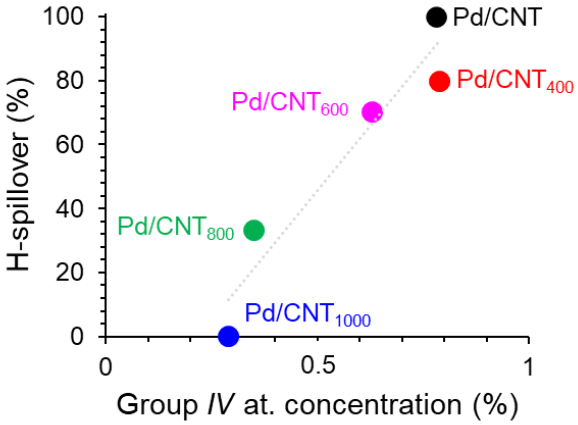

Figure 4. Correlations between the atomic surface concentration of the OFGs (type *IV*) determined by XPS (Table S6) and the extent of H-spillover.

To follow the H-spillover on the heat-treated samples, the same TPD experiment are conducted as for sample Pd/CNT (**Figure 2**). **Figure S14** shows the results obtained. No significant differences are noticed for the CO_2-TPD profiles (**Figure S14a**) and residual carboxylic and anhydride groups are detected on the four samples. After H_2 treatment, partial reduction of carboxylic groups to phenol are expected.[88] The Pd/CNT_{400} still contains significant amounts of carboxylic anhydrides and lactone groups, which have been proposed to be involved in H-spillover.[30] Lactones groups significantly decrease for the Pd/CNT_{600} and Pd/CNT_{800} samples. The presence of a peak at high temperature on the CO_2 profile of Pd/CNT_{1000} can be tentatively attributed to a Boudouard-type reaction.[88] The decrease of H-spillover for Pd/CNT_{800} and its complete disappearance for Pd/CNT_{1000} cannot be rationalized from the CO_2-TPD profiles only. Significant differences between samples Pd/CNT_{800} and Pd/CNT_{1000} and the other samples are visible on the CO-TPD profiles (**Figure S14b**). In particular, the peak centered at 700-800 °C corresponding to the phenol/semiquinone groups is significantly decreased in Pd/CNT_{800} and Pd/CNT_{1000} samples. Thus, it seems that the presence of residual groups of the carboxylic type is not sufficient to ensure the H-spillover. Since carbonyl groups have been identified as poorly efficient for H-spillover,[30] it can be proposed that the phenol and/or lactone groups, in combination with carboxylic groups, facilitate the H-spillover on the carbon supports. The H_2-TPD profiles of Pd/CNT_{400}, Pd/CNT_{600} and Pd/CNT_{1000} samples (**Figure S14c**) are quite similar. The Pd/CNT_{800} sample shows a higher amount of -CH functions, which could have been created during the reduction of this catalyst or during the experiment under H_2. The H_2O-

TPD profiles are similar for the four samples (**Figure S14d**). It is interesting to note that water is evolved at relatively low temperatures, and we should consider that water molecules can serves as shuttle for H species during the H-spillover.[96] To verify this hypothesis, the WO_3 reduction test was performed at 20 °C in the presence of water vapor with the Pd/CNT_{1000} sample that does not allow H-spillover. The results of these experiments are shown on **Figure S15**. Clearly, the presence of water vapor assisted the H-spillover on the carbon support. From the observed color change, the result obtained is similar to the Pd/CNT_{600} sample. In order to compare the efficiency between water-assisted and carboxyl-assisted H-spillover, a new Pd/CNT catalyst (Pd/CNT_p) was prepared, for which Pd was deposited on purified but not oxidized CNTs (CNT_p). As nitric acid oxidation is performed to introduce OFGs and particularly carboxylic groups, the CNT_p should contain few OFGs and no carboxylic groups. The resulting Pd/CNT_p has been characterized by ICP-OES, STEM-HAADF and XPS. The Pd loading (0.7 % w/w) is relatively low compared to the targeted value (1.2 % w/w), and the mean Pd particle size is 2.1 ± 0.7 nm (**Figure S16**). The XPS analysis (**Table S8**) shows that the Pd/CNT_p sample contains very few OFGs compared to the other samples. The measured C/O ratio is 56, whereas it lies between 20 and 27 for the other samples (**Table S6**). In addition, the Pd/CNT_p sample do not contain carboxylic groups (group *IV*). The H-spillover has been evaluated for this new sample in the presence or not of water (**Figure S17**). As expected, no H-spillover was observed in the absence of water, as for the Pd/CNT_{1000} sample, which contains very few carboxylic groups. No H-spillover was detected neither in the presence of water. This new result is important, since it shows that water-assisted H-spillover can be effective at room temperature only if enough carboxylic groups are present on the surface. Up to now, the positive role of water on H-spillover has been rationalized as followed: i) chemisorbed H atoms form strong C-H bonds with the support; ii) each chemisorbed H atom must form a pair with another H atom bound closely in order to lower the energy with respect to the free H_2 state; iii) because of the strong C-H bonds, the barrier for H cooperative migration is very high (> 46 $kcal.mol^{-1}$); and iv) when mediated by H_2O molecules, the barrier can be reduced to 20-30 $kcal.mol^{-1}$.[96-97] However, such barriers are not compatible with the fact that H-spillover can operate at room temperature. Our results demonstrate that for H-spillover to operate at room temperature, carboxylic groups should be present. If no carboxylic groups are present, H-spillover does not operate at room temperature, even in the presence of water. Consequently, at room temperature, the role of water should be to facilitate the H-spillover between carboxylic groups.

Finally, near-ambient pressure X-ray photoelectron spectroscopy (NAP-XPS) was performed to follow the H-spillover at room temperature on sample Pd/CNT_{400}. First, the XPS spectra were recorded under vacuum (experiment labeled "0") at room temperature. Then, individual data sets with O 1s and Pd 3d spectra at 1 mbar H_2 at room temperature were taken one after the other over for more than 2 hours (5 experiments labeled "1" to "5"). **Figure S18** shows the evolution of the high resolution Pd 3d and O 1s spectra. Some modifications of the Pd 3d and O 1s spectra can be noted upon H_2 introduction and at other intervals under H_2. The $Pd^{(0)}/Pd^{\delta+}$ ratio as well as the percentage of the various types of OFGs (types *I* to *IV*) was specifically followed and the evolution of these features is presented in **Figure S19**. The $Pd^{(0)}/Pd^{\delta+}$ ratio shows some fluctuations over time, with a slight tendency to increase (**Figure S19a**). The relative concentrations of the various types of oxygen species also shows fluctuations upon H_2 introduction and then over time at room temperature (**Fig. S19b**). For type *III* (phenol) and type *IV* (carboxylic) groups, there is a tendency over time for type *III* groups to decrease whereas type *IV* groups are increasing (**Fig. S19c**). The decreasing of phenolic group concentration over time might be related to the desorption of water.[17] The increase of carboxylic groups might be related to reaction of lactones with spilt-over H species.[33] Type *I* and *II* groups (carbonyl-containing groups) are not significantly impacted during the experiment (**Fig. S19d**). These last experimental results show that surface modifications occur during the H-spillover even at room temperature, affecting both the surface of palladium and that of the carbon support. It is interesting to note that at room temperature, these surface modifications are in the direction of an increase in the concentration of carboxylic groups, which we identified as key for the H-spillover.

3.2 Modeling study of H-spillover on a carbon supported Pd system

DFT simulations were conducted to provide insights into the H-spillover mechanism on TM-doped carbon materials. For this, a realistic model previously described by some of us was considered,[55] taking into account the greater proportion of basal planes (compared to prismatic planes) experimentally observed in CNTs, which essentially present graphene layers parallel to the axis of the tube. This model, representative of the Pd/CNT samples, integrates Pd particles (Pd_{NP}) and single atoms (Pd_{SA}) as metal species on a carbon support decorated with experimentally probed abundant OFGs (see section 3.1.1).

3.2.1 H_2 dissociative adsorption

The first step in the H-spillover process involves the coordination and subsequent dissociation of hydrogen molecules on Pd_{NP}.[77] In the absence of H atoms on the Pd_{NP} surface (H/Pd at. ratio = 0.00), H_2 is coordinated in top position (adsorption energy of -17.4 kcal·mol^{-1}, see **Figure S20**). The H–H distance turned out to be 0.88 Å (compared to 0.72 Å in the gas phase), so the molecule is clearly activated. The thermodynamics (reaction energy of -13.0 kcal·mol^{-1}) and the kinetics (energy barrier of 5.7 kcal·mol^{-1}) of the H_2 dissociation step indicated a very favorable and affordable process, leading to the formation of metal hydrides.[98] For a higher hydrogen coverage (H/Pd at. ratio = 0.92), a weaker adsorption energy is observed (-9.6 kcal·mol^{-1}, see **Figure S20**). At this hydrogen coverage, the dissociation reaction continues to be thermodynamically favorable, but kinetically slightly more restrained, -6.3 and 10.0 kcal·mol^{-1}, respectively. Thus, H_2 dissociative adsorption is feasible on small Pd_{NP} even at H/Pd at. ratios close to 1.0. As far as Pd_{SA} are concerned, H_2 can be adsorbed on the metal center; however, both homolytic and heterolytic H_2 dissociations being endothermic, they will not take place.[77] Consequently, these species should be considered as spectator in the first step of the H-spillover mechanism, even if they can act as receptors for H species.[74]

3.2.2 Hydrogen migration

The second step in the H-spillover process consists in the migration of hydrogen atoms from the metal to the support. The difficulty of this step for defect-free carbon materials is evident under standard conditions, since it is usually endothermic and requires overcoming energy barriers sometimes close to the desorption energy of the H atoms from the metallic species.[99] However, performance can be significantly improved when using defective or doped carbon materials.[100] Due to the HNO_3 oxidation of the carbon material, the Pd-doped carbon model presents three potential organic motifs in the vicinity of Pd_{NP} that can act as H-transfer groups: i) –COOH groups perpendicular to the carbon lattice; ii) –OH groups also perpendicular to the carbon lattice; and iii) –CO– groups located next to decorative vacancies.

The transfer *via* –COOH occurs through a concerted mechanism, in which one of the H atoms of the Pd_{NP} is transferred to the oxygen of the C=O fragment, while the H atom of the OH fragment migrates to the support. The flexibility of the acidic group due to C–C rotation and C–O–H bending facilitates the appropriate conformation for migrations (barrierless *cis-trans* isomerization of the –OH fragment). This allows H atoms to jump to various C atoms on the model support, as illustrated in **Figure 5a** and schematically represented in **Figure 5c**.

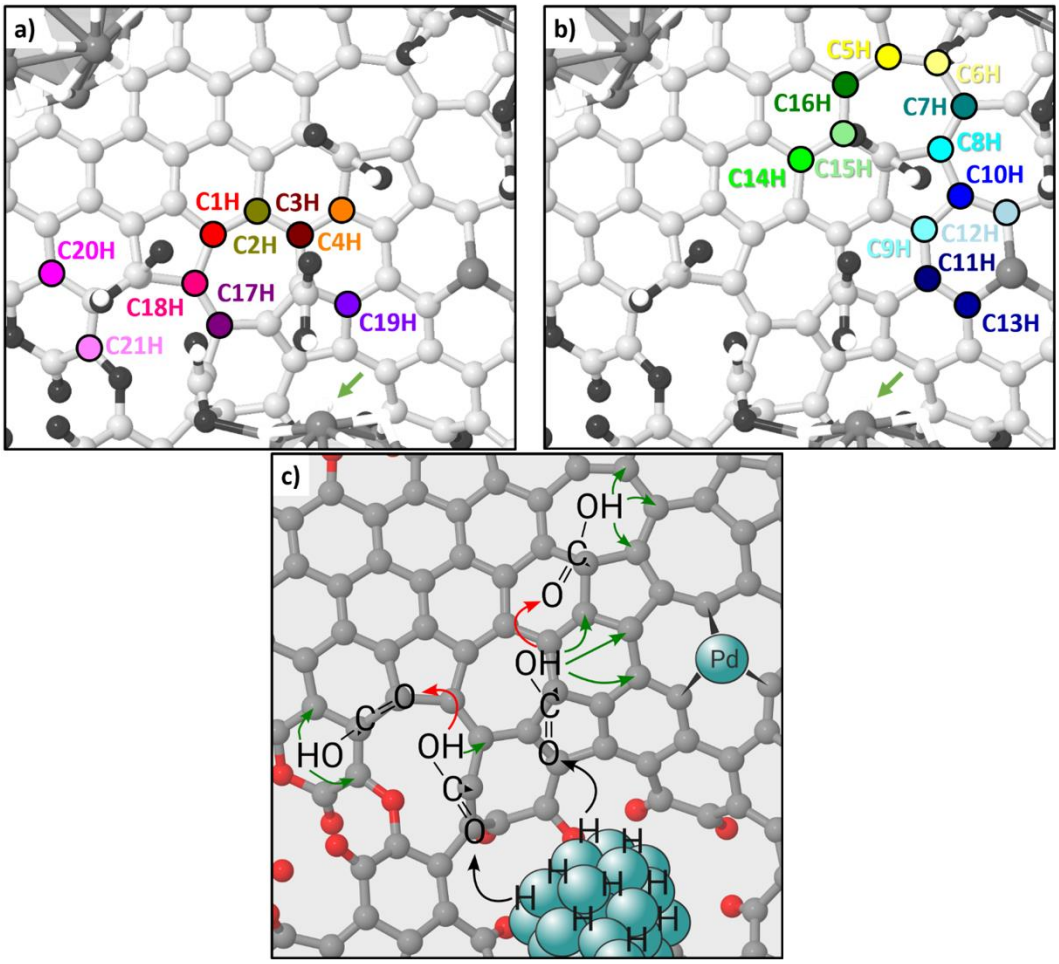

Figure 5. Illustration of potential sites for (a) hydrogen migration and (b) diffusion on the Pd-doped carbon model (each of them is labelled consecutively and represented with a different color). (c) Schematic representation of the key H-transfer steps involving the carboxylic groups, where the black arrow indicates from Pd_{NP} to –COOH, the red arrow indicates between –COOH, and the green arrows indicate from –COOH to the surface. Atomic color scheme: Pd (Sea Blue); O (Candy Apple Red); C (Philippine Gray); H (White).

The resulting energy profile along with their corresponding structures for the two most relevant sites is shown in **Figure 6** and for all positions in **Figure S21**. The *C3H* migration step (wine pathway) is thermodynamically favorable with an overall reaction energy of -12.6 kcal·mol^{-1}, whereas in the case of *C4H* (orange pathway) it is slightly unfavorable with a value of 3.1 kcal·mol^{-1}. Despite this significant difference in stability, the energy barriers are low and very similar for both pathways, between 13 and 15 kcal·mol^{-1}, which makes them affordable under experimental conditions. Charge analysis confirms the hydride to proton umpolung (or polarity inversion) of the transferred hydrogen atoms, with an average partial atomic charge of around -0.24, +0.51, and +0.36 |*e*| for the Pd_{NP}–H, COO–H, and C–H species, respectively. A detailed description of the bond lengths and charge distributions around the C–H groups can be seen in

Figure S22. It is interesting to note that the carboxyl groups coordinated with the Pd_{NP} are not able to participate in the H transfer process. The process involving polarity inversion, promoted by a low energy barrier in which the hydride in Pd_{NP}–H is the charge donor (ranging from negative to positive values) and the surface carbon atom that receives the hydrogen atom is the charge acceptor (ranging from positive or neutral values to negative), is in agreement with similar metallic systems reported in the literature.[101-102] Thus, the chemical nature of the diffusing hydrogen species can change significantly depending on which step of the spillover process is occurring and where they are located.

As an alternative to the concerted mechanism proposed for hydrogen transfer mediated by COOH groups, the possibility of a gradual mechanism was also considered, potentially involving the transfer of a hydrogen atom from *trans*–COOH to a neighboring carbon atom, and the subsequent CO_2 release. This novel hydrogen migration is evaluated using the same –COOH group and the same support carbon sites used previously, with the resulting energy profile along with their corresponding structures shown in **Figure S23**. Although a mechanism of this type is capable of offering more favorable thermodynamics for all cases than the concerted mechanism, with total reaction energies between -15 and -20 kcal·mol^{-1}, the kinetics are more impeded for all of them with energy barriers above 21 kcal·mol^{-1}. Thus, the release of CO_2 seems not to be competitive with the migration of hydrogen, as indicated by the experimental results with the characterization of stable carboxylic groups.

The initial model does not include phenolic/hydroxyl groups, although these could be present on the surface, since they are experimentally detected with the same TPD-MS signal as the ether groups. The extent of these –OH groups for hydrogen migration was evaluated by replacing the same –COOH group used previously for the migration step with a –OH one (the considered structure is provided in **Figure S24a**). The lower flexibility and bond length of this group makes migration infeasible, since the distance of 3.50 Å between the closest Pd_{NP}–H and the O–H fragment turns out to be unattainable.

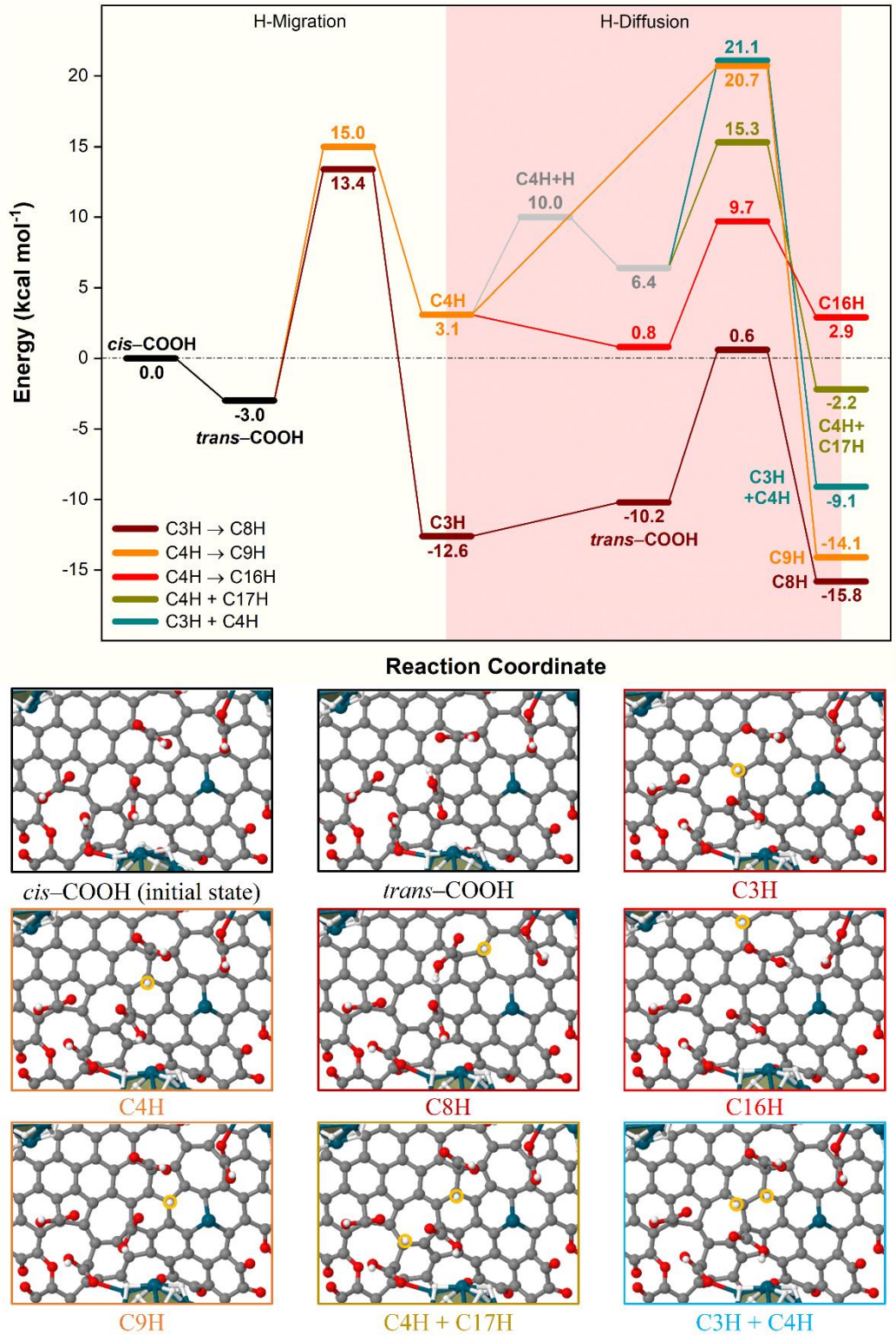

Figure 6. Reaction profile for the energetically most relevant sites (shown below as insets) of hydrogen migrations and diffusions (black and gray for the first and second common steps). Relative energies are referenced with respect to the carbon-supported Pd catalyst. Atomic color scheme: Pd (Sea Blue); O (Candy Apple Red); C (Philippine Gray); H (White).

Although it has been demonstrated that phenolic can be one of the dominant acidic sites in gas-phase chemistries,[103] the O-containing functional group has to be irremediably located at the edge of the graphitic carbon lattice (electron density delocalization induced by the neighboring aromatic rings conjugated with the conjugate base of the acidic site), which is not considered in this work.

Finally, the use of the C=O group as a transfer agent has also been considered (**Figure S25**). Interestingly, the transfer of an H from Pd_{NP} to the oxygen atom of the carbonyl group is more favorable than to a –COOH group from the thermodynamic and kinetic points of view (reaction energy of -40.8 *vs.* -12.6 kcal·mol^{-1} and energy barrier of 11.4 *vs.* 13.4 kcal·mol^{-1}, respectively). This is consistent with previous calculations showing that atomic H can bind very strongly to oxygen functionalities, such as to the basal-plane epoxide and edge carbonyl groups.[33] The distance between Pd_{NP}–H and the carbonyl O atom is 2.70 Å, very similar to 2.74 Å with the corresponding carboxyl O atom. An appreciably more hindered second H-spillover completes the carbonylic reduction to form hydroxylated CH–OH groups. The possibility of subsequent proton transfer through these new saturated species does not seem to be promoted due to the impossibility of delocalizing the electron density of the conjugate base from the potential acidic site with the aromatic ring to which it belongs. This implies that partially or fully saturated C=O groups can coexist in the vicinity of the metal catalyst, trapping hydrogen atoms.

Consequently, it is important to emphasize that –COOH groups located on the basal plane are the only OFGs capable of promoting hydrogen migration from the active metal species to the O-functionalized carbon support. The carbonyl groups decorating the metallic surroundings are more energetically prone, but the resulting reduced groups end up with a configuration (CH–OH) and a high stability, from which the H atoms can barely emerge. These results suggest that the H-spillover mechanism could progress: i) by migration of H atoms away from the Pd_{NP} through carboxyl groups; or ii) after reduction of all carbonyl groups around the Pd_{NP}.

3.2.3 Hydrogen diffusion

The final step considered in the H-spillover process encompasses the diffusion of hydrogen species on the support surface. The theoretical results raise the difficulty of chemisorbed H atoms, specially $H^{\delta-}$, moving freely at room temperature, since diffusion involves the dissociation of the C−H bond, with a relatively high activation energy (25-38 kcal·mol^{-1}).[104] Given the nature of the model support, H atoms can first diffuse over a short range directly to other adjacent carbon atoms (see **Figure 5b**). Starting from the thermodynamically most

favorable *C3H* position, the two possible hopping to the two neighboring carbons (*i.e.*, the *C2H* and *C4H* positions) resulted in endothermic and moderately costly processes at room temperature (average reaction energies and energy barriers of around 16 and above 32 kcal·mol^{-1}, see **Figure S26**), in agreement with what was reported for the H diffusion on CNTs and polyaromatic carbon materials.[104] In contrast, the migration of hydrogen from the *C4H* position to the *C3H* and *C9H* positions turned out to be clearly exothermic, with reaction energies greater than -15.8 kcal·mol^{-1}, mainly due to the slight endothermy shown by the starting position (see **Figure S27**). The latter (*C9H*), with an energy barrier of 17.6 kcal·mol^{-1}, was kinetically more enabled (by 3.8 kcal·mol^{-1}) than the former (*C3H*), as shown with the *C4H* → *C9H* diffusion step (in orange) in **Figure 6**. However, from *C4H* the H-diffusion appears to be non-competitive with respect to the back H-migration due to a lower barrier (11.9 *vs.* 17.6 kcal·mol^{-1}) of the back H-migration process. Thus, from *C4H*, the migration process leading to the initial *trans*–COOH state is faster than the diffusion process to form the *C5H* product. As the *C9H* product is more thermodynamically stable, it is possible that more drastic reaction conditions could give rise to the hydrogen diffusion pathway through the carbon lattice. It is interesting to note that *C9H* is found in the vicinity of a single Pd atom in a single vacancy, a species of great interest in selective hydrogenation reactions of organic substrates.[105] The H atom could reach the Pd_{SA} from this position (*para* with respect to the metal) in a single step or by cascade diffusion through the *meta* and *ortho* relative positions. In any case, neither of the two paths seems to lead preferentially to the hydrogenated metal species Pd_{SA}–H, mainly due to the high thermodynamic stability (at -14.1 kcal·mol^{-1}) of the *C9H* position (both diffusion pathways are illustrated in **Figure S28**).

Hydrogen diffusion became more effective in the medium/long-range using the numerous acidic functionalities available on the model carbon support. As in the migration step, the carboxyl groups manage to reduce energy costs by simultaneously transferring the H atom from the support to the C=O fragment and the H atom from the O–H fragment back to the surface (as shown in **Figure 5b** and schematically represented in **Figure 5c**). Thus, while thermodynamics showed values close to thermoneutrality for the most favorable diffusion processes from the *C3H* position (see **Figure S29**), the kinetics revealed energy barriers accessible under experimental conditions, as illustrated in **Figure 6** (in wine) with the *C8H* position (effective reaction energy and energy barrier of -3.2 and 13.2 kcal·mol^{-1}). The H-diffusion from the *C4H* position was also possible, being less favorable thermodynamically (reaction energy of 2.1 kcal·mol^{-1}) but kinetically more feasible (energy barrier of 8.9 kcal·mol^{-}

[1]) than the unassisted direct diffusion of hydrogen, as represented in **Figure 6** and **S30**, with position *C16H* (in red). Finally, COOH-assisted H diffusion was unfavorable in the case of *C9H* (average reaction energies and energy barriers above 14 and around 26 kcal·mol^{-1}, respectively, see **Figure S31**), which could indicate that if an H atom arrived on a carbon with this particular configuration, it would almost be trapped so as not to continue undergoing H-spillover. This specific configuration (H atom in *para* position with respect to the Pd_{SA} anchored in a single vacancy) has recently been proposed by some of us as a potential active species contributing to the selective hydrogenation of phenylacetylene directly.[105] Thus, in contrast to the unassisted hydrogen diffusion pathway, the carboxyl group-assisted H-diffusion pathway appears to be kinetically favorable regardless of the migration position of *C3H* or *C4H* (except the *C9H* position). Consequently, the role of –COOH functional groups continues to be essential throughout the different steps of the H-spillover mechanism.

In addition, as modeled for the hydrogen migration step, the –COOH group previously used as an assistant was replaced by an –OH group to assess its capability in the H-diffusion step (the atomistic model is depicted in **Figure S24b**). Regardless of the starting *C3H* or *C4H* migration position, the hydroxyl group was mostly inefficient for potential diffusion processes between carbons (see **Figure S32** and **S33**). The reaction energies were relatively comparable for –COOH- and –OH-assisted hydrogen hopping, with values close to thermoneutrality. However, the energy barriers with hydroxyl were much higher than with carboxyl due to the need for excessive bending. Only one exception is observed (*C4H* → *C8H* H-diffusion) for which the energy barrier of 23.7 kcal·mol^{-1} is accessible under experimental conditions. In this case, the H diffusion takes place between carbon atoms adjacent to the one carrying the hydroxyl group. Therefore, the assistance of hydroxyl functional groups in the hydrogen diffusion between carbons seems restricted and, consequently, less important than that of carboxyl groups, although their presence in carbon materials might contribute to the H-spillover mechanism by diffusing an H atom from an –OH group to an adjacent O (epoxide) atom.[17]

Instead of diffusion of hydrogen species on carbon materials, a second H migration from Pd_{NP} could take place after the first one (see **Figure 5a**). Larger hydrogen island structures may be formed by saturating the support after sequential addition of H atoms because of faster kinetics for migration than for diffusion.[106] From the *C3H* or *C9H* positions, none of the many possible processes was energetically viable due to kinetic impediments (energy barriers above 29 kcal·mol^{-1}, see **Figure S34** and **S36**). However, the *C4H* position enhanced access to a second migration, particularly the *C4H*– *C17H* (in green) and *C3H*–*C4H* (in dark cyan) pathways, as

shown in **Figure 6** (the other H migrations are revealed in **Figure S35**). The difference between these two intermediates is the H-location, in the first case being far from each other (about 4.42 Å) and in the second case attached to two adjacent carbon atoms in a geminal position (around 2.12 Å). Thus, for *C4H– C17H*, the two transferred H atoms can be considered as two independent C–H entities, being able to undergo diffusion processes that can eventually lead to the *C3H–C4H* scenario. The *C3H–C4H* configuration, reminiscent of a double bond hydrogenation, was found to be very stable, preventing most surface processes, such as simple (one at a time) or coupled (both at once) diffusion, –COOH group-assisted diffusion, H_2 recombination, and even a third H migration (the energetics are found in **Figure S37**-**S39**). For all these reasons, the presence of small areas of saturated graphite during H-spillover phenomena would be feasible, as confirmed by the TPD experiments. However, the concerted or assisted migration of H atoms from these areas is complicated from a kinetic point of view and most of the time endothermic from a thermodynamic point of view.

3.2.4 Importance of water

The experimental results showed that the surface composition of the carbon material changed as the H-spillover phenomenon progressed, highlighting the formation of water. The water formed (or other protic species) can be used to activate C–H bonds on the surface of the carbon material, as demonstrated in previous studies.[96-97] To computationally rationalize the positive role of water as a possible shuttle for H species, an explicit water molecule was included in the model support, positioned between the participating carboxylic groups to maximize hydrogen bonding interactions. The use of a single water molecule as an explicit solvent gives rise to an incipient illustration of the influence of the solvent. Due to a relatively small space between the Pd_{NP} and the carboxylic group, and only traces of water experimentally present, there would be no need to resort to liquid water models (implicit solvent) around the active sites. Thus, the spillover mechanism would take place by transferring the H atom from Pd_{NP} to the water molecule through a first –COOH group, and subsequently to the support along a second carboxylic group, as illustrated in **Figure 5a**. The resulting energy profiles along with the corresponding structures are summarized in **Figure S40** and **S41**. The placement of the water molecule allows the H species to be directed toward a graphitic-like region (**Figure S40**) or a more oxidized region (**Figure S41**), the results showing a clear preference for the hydrogenation of surface carbons on the graphitic-like regions. This is consistent with the aforementioned difficulty in saturating C atoms bonded to O atoms, which could lead to routing H-spillover through less O-functionalized carbon-based regions. Interestingly, among the different

possibilities for accommodating the spilt-over hydrogen, the *C8H*^{w2} position (light blue pathway in **Figure 7**) turned out to be the most plausible. It is located in geminal position to a –COOH group in a Stone-Wales point defect with a "577" carbon rearrangement. This position also corresponds to the most probable H-diffusion in the absence of water. By comparing in **Figure 7** the predominant mechanisms of H-spillover (including hydrogen migration and co-diffusion) in the presence or absence of water, it is possible to highlight the role of H_2O.

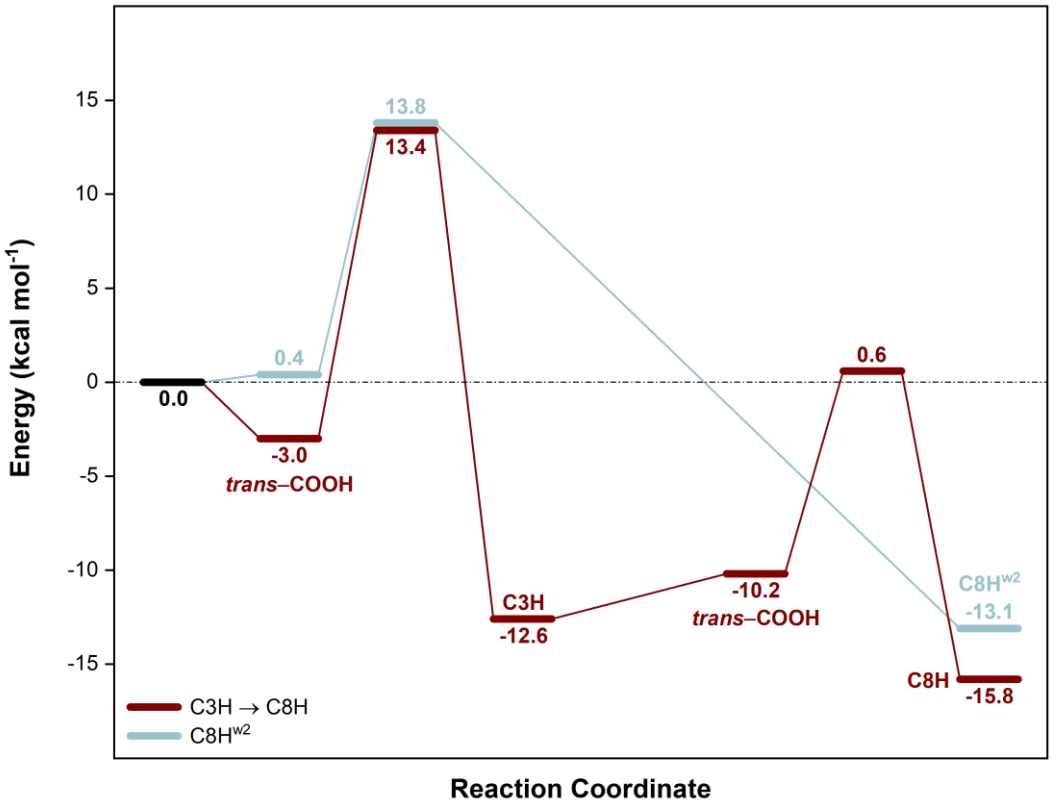

Figure 7. Reaction profile of non-assisted (*C3H→ C8H*) and water assisted (*C8H*^{w2}) hydrogen migration and co-diffusion. Relative energies are referenced with respect to the carbon-supported Pd catalyst (+ $H_2O_{(g)}$).

Both pathways appear to have quite similar favorable thermodynamic and kinetic contributions, with minor energetic differences (2.7 kcal·mol^{-1}). However, from a kinetic perspective, the H_2O-assisted mechanism evolves in a single energy barrier slightly below (2.6 kcal·mol^{-1}) the most energy-demanding step of the mechanism in the absence of water, corresponding to H-migration. This would significantly facilitate the migration of H atoms and would thus point to a faster kinetics of the H-spillover phenomenon in the presence of water.[96-97] Additionally, water could avoid potential resting states such as the *C3H* position, so it would be possible to

chain successive hydrogen transfer steps between water molecules and –COOH functional groups.[107]

4. Conclusion

This study, combining experiment and modeling, allowed progressing in the understanding of the H-spillover mechanism on carbon materials. A series of palladium-doped carbon nanotubes presenting Pd_{NP} and Pd_{SA}, as well as different concentrations and types of surface oxygen groups, were prepared and characterized. H-spillover was experimentally probed and quantified in the series of Pd-doped CNT. Systematic characterizations by XPS and TPD reveal that concentrations and types of OFGs are modified by H-spillover. The reaction temperature has a pronounced effect on the type of transformations observed. At room temperature, NAP-XPS experiments have shown that carboxylic groups are created whereas phenol groups are consumed. At higher temperature (in this case 150 °C), the TPD experiment reveals that the less stable CO_2-releasing groups are consumed. The XPS and TPD results also evidence that the carboxylic groups on the carbon material play a crucial role in the H-spillover to proceed. The combination of carboxylic and phenol and/or lactone groups could also be efficient, although to a lesser extent. Considering the model proposed by Koren and Soffer for H-spillover on carbon surfaces,[23] where the OFGs (and adsorbed water) serve as electrolyte for protonic conduction, our findings show that surface ionic conductivity can be assured only if a sufficient density of surface carboxylic groups is present on the surface. A model integrating Pd_{SA} and Pd_{NP} on an oxidized carbon support was built to validate the experimental study through modeling. This model first served as the basis for a theoretical study on molecular hydrogen activation on Pd_{NP}, showing an affordable process. The modeling study of H-spillover on Pd-doped carbon has demonstrated the feasibility of the process. The simulations confirm: i) the need for surface carboxylic groups for H migration to trigger the spillover process, and ii) that these carboxylic groups can also work in combination with phenol groups to facilitate H-spillover on the carbon support. Finally, the positive role of water, which act in concert with carboxylic groups at ambient temperature, on H-spillover was also highlighted experimentally and theoretically. These results provide a molecular scale understanding of one of the positive role of water often observed during hydrogenation reactions over carbon-supported catalysts,[108] because the H species resulting from H-spillover can be directly be involved in the hydrogenation steps of some substrates,[109] as it is the case for oxide supports.[9] These results emphasize the importance of rational surface modification of carbon materials to regulate the

H-spillover. Precise syntheses should be developed to go in that direction, so as to be able to regulate H-spillover strength for enhanced catalytic performance.[110-111] This study also show how surface chemistry affects and is affected by H-spillover. Consideration of these different elements should allow significant advances in the field of catalytic reactions involving hydrogen and, in a broader context, for the hydrogen-based economy.

▪ ASSOCIATED CONTENT

AUTHOR INFORMATION

Corresponding Author

*E-mail: philippe.serp@ensiacet.fr; igerber@insa-toulouse.fr

ORCID

Javier Navarro-Ruiz: orcid.org/0000-0002-3604-9338

Jérémy Audevard: orcid.org/0000-0002-8243-9556

Mathieu Vidal: https://orcid.org/0009-0008-8430-9035

Cristian H. Campos: https://orcid.org/0000-0001-8592-5384

Iker del Rosal: orcid.org/0000-0001-6898-4550

Philippe Serp: orcid.org/0000-0003-1424-2724

Iann C. Gerber: orcid.org/0000-0001-5091-2655

Author Contributions

The manuscript was written through contributions of all authors. All authors have given approval to the final version of the manuscript.

Funding Sources

This work has received funding from the French Agence Nationale de la Recherche under grant agreement ANR-19-CE07-0030 (COMET) and ANR-21-CE07-0021 (GRAAL). This work was also supported by ECOS Sud - ANID (project ECOS n° C21E03).

NOTES

The authors declare no competing financial interest.

Supporting Information

Structural properties, SEM, TEM, HRTEM, XPS (C 1s), TPD-MS (CO and CO_2), and surface density of CNT support; STEM-HAADF and particle size distributions of Pd-doped CNT; TPD (CO_2, CO, H_2, and H_2O) of CNT and Pd-doped CNT; TPD (CO and CO_2) of CNT and CNT_{400}; XPS (O 1s) of CNT_{400}, CNT_{600}, CNT_{800}, and CNT_{1000}; STEM, STEM-HAADF, particle size distributions, and XPS (O 1s and Pd 3d) of Pd/CNT_{400}, Pd/CNT_{600}, Pd/CNT_{800}, and Pd/CNT_{1000}; UV-Vis spectra of the resulting WO_3 + Pd/CNTs powders; hydrogen spillover quantification; correlations between the atomic surface concentration of OFGs and the extent of H-spillover; XPS (Pd 3d and O 1s) evolution of Pd/CNT_{400} under H_2; evolution of $Pd^{(0)}/Pd^{\delta+}$ ratio and types of OFGs during NAP-XPS; reaction profiles (and corresponding structures) of H_2 dissociative adsorption on Pd_{NP} and H-migrations from Pd_{NP} *via* –COOH and *via* C=O; bond lengths and charge distributions around the C–H groups; model carbon supports including –OH; reaction profiles of H-diffusions and second H-migrations from *C3H*, *C4H*, and *C9H* positions; reaction profiles of simple and coupled H diffusions (*via* the carbon support itself and *via* –COOH), H_2 recombination, and third H migration from *C50H* + *C68H* position; reaction profiles of H-diffusions *via* –OH from *C3H* and *C4H* positions; and reaction profiles of H-migration and co-diffusions *via* water and –COOH.

ACKNOWLEDGMENTS

We acknowledge financial support for this work from the French Agence Nationale de la Recherche under grant agreement ANR-19-CE07-0030 (COMET) and ANR-21-CE07-0021 (GRAAL). This work was also supported by ECOS Sud - ANID (project ECOS n° C21E03). J.N.-R., I.d.R., and I.C.G. thankfully acknowledge the computer resources through the “Calcul en Midi-Pyrénées” initiative CALMIP (projects p0812 and p1214), and CINES, IDRIS, and TGCC under the allocation 2022-A0120906649 made by GENCI. Dr. Paul Dietrich from

SPECS Surface Nano Analysis GmbH (Berlin, Germany) is acknowledged for measuring the samples by NAP-XPS (EnviroESCA instrument). Dr. Tobias Placke (Mercedes-Benz AG) is acknowledged for DFT calculations derived from N_2 adsorption data performed in MEET Battery Research Center, University of Münster (Germany).

REFERENCES

1. Prins, R., Hydrogen Spillover. Facts and Fiction. *Chem. Rev.* **2012,** *112* (5), 2714-2738.

2. Boudart, M.; Vannice, M. A.; Benson, J. E., Adlineation, Portholes and Spillover. *Z. Phys. Chem.* **1969**, *64*, 171-177.

3. Kohn, H. W.; Boudart, M., Reaction of Hydrogen with Oxygen Adsorbed on a Platinum Catalyst. *Science* **1964,** *145* (3628), 149-150.

4. Li, M.; Yin, W.; Pan, J.; Zhu, Y.; Sun, N.; Zhang, X.; Wan, Y.; Luo, Z.; Yi, L.; Wang, L., Hydrogen spillover as a promising strategy for boosting heterogeneous catalysis and hydrogen storage. *Chem. Eng. J.***2023,** *471*, 144691.

5. Chen, Y.; Zheng, W.; Chen, M.; Guan, X., Role of Hydrogen Spillover in Electrocatalytic Hydrogen Evolution from Water Splitting. In *Transition Metal-Based Electrocatalysts: Applications in Green Hydrogen Production and Storage*, American Chemical Society: 2023; Vol. 1435, pp 147-168.

6. Bettahar, M. M., The hydrogen spillover effect. A misunderstanding story. *Catal. Rev.* **2022,** *64* (1), 87-125.

7. Karim, W.; Spreafico, C.; Kleibert, A.; Gobrecht, J.; VandeVondele, J.; Ekinci, Y.; van Bokhoven, J. A., Catalyst support effects on hydrogen spillover. *Nature* **2017,** *541* (7635), 68-71.

8. Pyle, D. S.; Gray, E. M.; Webb, C. J., Hydrogen storage in carbon nanostructures via spillover. *Int. J. Hydrogen Energy.* **2016,** *41* (42), 19098-19113.

9. Merte, L. R.; Peng, G.; Bechstein, R.; Rieboldt, F.; Farberow, C. A.; Grabow, L. C.; Kudernatsch, W.; Wendt, S.; Lægsgaard, E.; Mavrikakis, M.; Besenbacher, F., Water-Mediated Proton Hopping on an Iron Oxide Surface. *Science* **2012,** *336* (6083), 889-893.

10. Gu, Z.; Li, M.; Chen, C.; Zhang, X.; Luo, C.; Yin, Y.; Su, R.; Zhang, S.; Shen, Y.; Fu, Y.; Zhang, W.; Huo, F., Water-assisted hydrogen spillover in Pt nanoparticle-based metal–organic framework composites. *Nat. Commun.* **2023,** *14* (1), 5836.

11. Wu, S.; Tseng, K.-Y.; Kato, R.; Wu, T.-S.; Large, A.; Peng, Y.-K.; Xiang, W.; Fang, H.; Mo, J.; Wilkinson, I.; Soo, Y.-L.; Held, G.; Suenaga, K.; Li, T.; Chen, H.-Y. T.; Tsang, S.

C. E., Rapid Interchangeable Hydrogen, Hydride, and Proton Species at the Interface of Transition Metal Atom on Oxide Surface. *J. Am. Chem. Soc.* **2021,** *143* (24), 9105-9112.

12. Choi, M.; Yook, S.; Kim, H., Hydrogen Spillover in Encapsulated Metal Catalysts: New Opportunities for Designing Advanced Hydroprocessing Catalysts. *ChemCatChem* **2015,** *7* (7), 1048-1057.

13. Itoi, H.; Kameoka, S.; Matsuoka, C.; Goto, Y.; Miyaji, M.; Ohmi, H.; Miyake, S.; Ishii, T.; Iwata, H.; Ohzawa, Y., Macroscopic Study on the Behavior of Spillover Hydrogen Atoms. *J. Phys. Chem. C* **2023,** *127* (30), 14723-14732.

14. Robell, A. J.; Ballou, E. V.; Boudart, M., Surface Diffusion of Hydrogen on Carbon. *J. Phys. Chem.* **1964,** *68* (10), 2748-2753.

15. D'Anna, V.; Duca, D.; Ferrante, F.; La Manna, G., DFT studies on catalytic properties of isolated and carbon nanotube supported Pd_9 cluster–I: adsorption, fragmentation and diffusion of hydrogen. *Phys. Chem. Chem. Phys.* **2009,** *11* (20), 4077-4083.

16. Alonso, J. A.; López, M. J., Interaction of Hydrogen with Graphitic Surfaces, Clean and Doped with Metal Clusters. In *Handbook of Materials Modeling: Applications: Current and Emerging Materials*, Andreoni, W.; Yip, S., Eds. Springer International Publishing: Cham, 2018; pp 1-22.

17. Psofogiannakis, G. M.; Froudakis, G. E., DFT Study of Hydrogen Storage by Spillover on Graphite with Oxygen Surface Groups. *J. Am. Chem. Soc.* **2009,** *131* (42), 15133-15135.

18. Psofogiannakis, G. M.; Froudakis, G. E., Fundamental studies and perceptions on the spillover mechanism for hydrogen storage. *Chem. Commun.* **2011,** *47* (28), 7933-7943.

19. Juarez-Mosqueda, R.; Mavrandonakis, A.; Kuc, A. B.; Pettersson, L. G. M.; Heine, T., Theoretical analysis of hydrogen spillover mechanism on carbon nanotubes. *Front. Chem.* **2015,** *3* (2).

20. Psofogiannakis, G. M.; Froudakis, G. E., DFT Study of the Hydrogen Spillover Mechanism on Pt-Doped Graphite. *J. Phys. Chem. C* **2009,** *113* (33), 14908-14915.

21. Yang, F.; Hu, B.; Xia, W.; Peng, B.; Shen, J.; Muhler, M., On the nature of spillover hydrogen species on platinum/nitrogen-doped mesoporous carbon composites: A temperature-programmed nitrobenzene desorption study. *J. Catal.* **2018,** *365*, 55-62.

22. Shun, K.; Mori, K.; Masuda, S.; Hashimoto, N.; Hinuma, Y.; Kobayashi, H.; Yamashita, H., Revealing hydrogen spillover pathways in reducible metal oxides. *Chem. Sci.* **2022,** *13* (27), 8137-8147.

23. Keren, E.; Soffer, A., Simultaneous electronic and ionic surface conduction of catalyst supports: A general mechanism for spillover: The role of water in the Pd-catalyzed hydrogenation of a carbon surface. *J. Catal.* **1977,** *50* (1), 43-55.

24. Tan, M.; Yang, Y.; Yang, Y.; Chen, J.; Zhang, Z.; Fu, G.; Lin, J.; Wan, S.; Wang, S.; Wang, Y., Hydrogen spillover assisted by oxygenate molecules over nonreducible oxides. *Nat. Commun.* **2022,** *13* (1), 1457.

25. Fischer, A. F.; Iglesia, E., The nature of "hydrogen spillover": Site proximity effects and gaseous intermediates in hydrogenation reactions mediated by inhibitor-scavenging mechanisms. *J. Catal.* **2023,** *420*, 68-88.

26. Bhat, V. V.; Contescu, C. I.; Gallego, N. C., The role of destabilization of palladium hydride in the hydrogen uptake of Pd-containing activated carbons. *Nanotechnology* **2009,** *20* (20), 204011.

27. Casartelli, M.; Casolo, S.; Tantardini, G. F.; Martinazzo, R., Structure and stability of hydrogenated carbon atom vacancies in graphene. *Carbon* **2014,** *77*, 165-174.

28. Chen, L.; Pez, G.; Cooper, A. C.; Cheng, H., A mechanistic study of hydrogen spillover in MoO3 and carbon-based graphitic materials. *J. Condens. Matter Phys.* **2008,** *20* (6), 064223.

29. Dong Jin, S.; Tae-Jin, P.; Son-Ki, I., Effect of surface oxygen groups of carbon supports on the characteristics of Pd/C catalysts. *Carbon* **1993,** *31* (3), 427-435.

30. Badenes, P.; Daza, L.; Rodriguez-Ramos, I.; Guerrero-Ruiz, A., Mechanism of hydrogen spillover over carbon supported metal catalysts. In *Studies in Surface Science and Catalysis*, Li, C.; Xin, Q., Eds. Elsevier: 1997; Vol. 112, pp 241-250.

31. Li, Q.; Lueking, A. D., Effect of Surface Oxygen Groups and Water on Hydrogen Spillover in Pt-Doped Activated Carbon. *J. Phys. Chem. C* **2011,** *115* (10), 4273-4282.

32. Parambhath, V. B.; Nagar, R.; Sethupathi, K.; Ramaprabhu, S., Investigation of Spillover Mechanism in Palladium Decorated Hydrogen Exfoliated Functionalized Graphene. *J. Phys. Chem. C* **2011,** *115* (31), 15679-15685.

33. Wang, Z.; Yang, F. H.; Yang, R. T., Enhanced Hydrogen Spillover on Carbon Surfaces Modified by Oxygen Plasma. *J. Phys. Chem. C* **2010,** *114* (3), 1601-1609.

34. García-García, F. R.; Bion, N.; Duprez, D.; Rodríguez-Ramos, I.; Guerrero-Ruiz, A., H2/D2 isotopic exchange: A tool to characterize complex hydrogen interaction with carbon-supported ruthenium catalysts. *Catal. Today* **2016,** *259*, 9-18.

35. Anbia, M.; Mandegarzad, S., Enhanced hydrogen sorption on modified MIL-101 with Pt/CMK-3 by hydrogen spillover effect. *J. Alloys Compd.* **2012,** *532*, 61-67.

36. Li, Q.; Wang, H.; Xia, H.; Wei, S.; Yang, J., Density functional study of hydrogen adsorption and diffusion on Ni-loaded graphene and graphene oxide. *Int. J. Quantum Chem.* **2014,** *114* (13), 879-884.

37. Das, T. K.; Banerjee, S.; Pandey, M.; Vishwanadh, B.; Kshirsagar, R. J.; Sudarsan, V., Effect of surface functional groups on hydrogen adsorption properties of Pd dispersed reduced graphene oxide. *Int. J. Hydrogen Energy.* **2017,** *42* (12), 8032-8041.

38. Wang, L.; Yang, R. T., Molecular hydrogen and spiltover hydrogen storage on high surface area carbon sorbents. *Carbon* **2012,** *50* (9), 3134-3140.

39. Tsao, C.-S.; Liu, Y.; Chuang, H.-Y.; Tseng, H.-H.; Chen, T.-Y.; Chen, C.-H.; Yu, M.-S.; Li, Q.; Lueking, A.; Chen, S.-H., Hydrogen Spillover Effect of Pt-Doped Activated Carbon Studied by Inelastic Neutron Scattering. *J. Phys. Chem. Lett.* **2011,** *2* (18), 2322-2325.

40. Geng, Z.; Wang, D.; Zhang, C.; Zhou, X.; Xin, H.; Liu, X.; Cai, M., Spillover enhanced hydrogen uptake of Pt/Pd doped corncob-derived activated carbon with ultra-high surface area at high pressure. *Int. J. Hydrogen Energy.* **2014,** *39* (25), 13643-13649.

41. Broom, D. P.; Hirscher, M., Irreproducibility in hydrogen storage material research. *Energy Environ. Sci.* **2016,** *9* (11), 3368-3380.

42. Contreras, R. C.; Guicheret, B.; Machado, B. F.; Rivera-Cárcamo, C.; Curiel Alvarez, M. A.; Valdez Salas, B.; Ruttert, M.; Placke, T.; Favre Réguillon, A.; Vanoye, L.; de Bellefon, C.; Philippe, R.; Serp, P., Effect of mesoporous carbon support nature and pretreatments on palladium loading, dispersion and apparent catalytic activity in hydrogenation of myrcene. *J. Catal.* **2019,** *372*, 226-244.

43. Dietrich, P. M.; Bahr, S.; Yamamoto, T.; Meyer, M.; Thissen, A., Chemical surface analysis on materials and devices under functional conditions – Environmental photoelectron spectroscopy as non-destructive tool for routine characterization. *J. Electron Spectrosc. Relat. Phenom.* **2019,** *231*, 118-126.

44. Arinchtein, A.; Schmack, R.; Kraffert, K.; Radnik, J.; Dietrich, P.; Sachse, R.; Kraehnert, R., Role of Water in Phase Transformations and Crystallization of Ferrihydrite and Hematite. *ACS Appl. Mater. Interfaces* **2020,** *12* (34), 38714-38722.

45. Kuo, C.-T.; Lu, Y.; Kovarik, L.; Engelhard, M.; Karim, A. M., Structure Sensitivity of Acetylene Semi-Hydrogenation on Pt Single Atoms and Subnanometer Clusters. *ACS Catal.* **2019,** *9* (12), 11030-11041.

46. Borodziński, A.; Bonarowska, M., Relation between Crystallite Size and Dispersion on Supported Metal Catalysts. *Langmuir* **1997,** *13* (21), 5613-5620.

47. Olivier, J. P.; Winter, M., Determination of the absolute and relative extents of basal plane surface area and “non-basal plane surface” area of graphites and their impact on anode performance in lithium ion batteries. *J. Power Sources* **2001,** *97-98*, 151-155.

48. Placke, T.; Siozios, V.; Rothermel, S.; Meister, P.; Colle, C.; Winter, M., Assessment of Surface Heterogeneity: a Route to Correlate and Quantify the 1st Cycle Irreversible Capacity Caused by SEI Formation to the Various Surfaces of Graphite Anodes for Lithium Ion Cells. *Z. Phys. Chem.* **2015,** *229* (9), 1451-1469.

49. Kresse, G.; Furthmüller, J., Efficiency of ab-initio total energy calculations for metals and semiconductors using a plane-wave basis set. *Comput. Mater. Sci.* **1996,** *6* (1), 15-50.

50. Kresse, G.; Furthmüller, J., Efficient iterative schemes for ab initio total-energy calculations using a plane-wave basis set. *Phys. Rev. B* **1996,** *54* (16), 11169-11186.

51. Perdew, J. P.; Burke, K.; Ernzerhof, M., Generalized Gradient Approximation Made Simple. *Phys. Rev. Lett.* **1996,** *77* (18), 3865-3868.

52. Grimme, S.; Antony, J.; Ehrlich, S.; Krieg, H., A consistent and accurate ab initio parametrization of density functional dispersion correction (DFT-D) for the 94 elements H-Pu. *J. Chem. Phys.* **2010,** *132* (15).

53. Blöchl, P. E., Projector augmented-wave method. *Phys. Rev. B* **1994,** *50* (24), 17953-17979.

54. Kresse, G.; Joubert, D., From ultrasoft pseudopotentials to the projector augmented-wave method. *Phys. Rev. B* **1999,** *59* (3), 1758-1775.

55. Navarro-Ruiz, J.; Rivera-Cárcamo, C.; Machado, B.; Serp, P.; Del Rosal, I.; Gerber, I. C., Computational Design of Pd Nanoclusters and Pd Single-Atom Catalysts Supported on O-Functionalized Graphene. *ACS Appl. Nano Mater.* **2021,** *4* (11), 12235-12249.

56. Monkhorst, H. J.; Pack, J. D., Special points for Brillouin-zone integrations. *Phys. Rev. B* **1976,** *13* (12), 5188-5192.

57. Makov, G.; Payne, M. C., Periodic boundary conditions in ab initio calculations. *Phys. Rev. B* **1995,** *51* (7), 4014-4022.

58. Henkelman, G.; Jónsson, H., Improved tangent estimate in the nudged elastic band method for finding minimum energy paths and saddle points. *J. Chem. Phys.* **2000,** *113* (22), 9978-9985.

59. Henkelman, G.; Uberuaga, B. P.; Jónsson, H., A climbing image nudged elastic band method for finding saddle points and minimum energy paths. *J. Chem. Phys.* **2000,** *113* (22), 9901-9904.

60. Cançado, L. G.; Jorio, A.; Ferreira, E. H. M.; Stavale, F.; Achete, C. A.; Capaz, R. B.; Moutinho, M. V. O.; Lombardo, A.; Kulmala, T. S.; Ferrari, A. C., Quantifying Defects in Graphene via Raman Spectroscopy at Different Excitation Energies. *Nano Lett.* **2011,** *11* (8), 3190-3196.

61. Lee, S.-H.; Hwang, Y.-M.; Byun, T.-S.; Ko, J.-H.; Roh, J.-S., Effect of heating rate, temperature, and residence time during graphitization on the mechanical and electrical properties of isotropic graphite blocks. *Carbon* **2023,** *208*, 443-451.

62. Darmstadt, H.; Roy, C., Surface spectroscopic study of basic sites on carbon blacks. *Carbon* **2003,** *41* (13), 2662-2665.

63. Smith, M.; Scudiero, L.; Espinal, J.; McEwen, J.-S.; Garcia-Perez, M., Improving the deconvolution and interpretation of XPS spectra from chars by ab initio calculations. *Carbon* **2016,** *110*, 155-171.

64. Brender, P.; Gadiou, R.; Rietsch, J.-C.; Fioux, P.; Dentzer, J.; Ponche, A.; Vix-Guterl, C., Characterization of Carbon Surface Chemistry by Combined Temperature Programmed Desorption with in Situ X-ray Photoelectron Spectrometry and Temperature Programmed Desorption with Mass Spectrometry Analysis. *Anal. Chem.* **2012,** *84* (5), 2147-2153.

65. Godino-Salido, M. L.; López-Garzón, R.; Gutiérrez-Valero, M. D.; Arranz-Mascarós, P.; Melguizo-Guijarro, M.; López de la Torre, M. D.; Gómez-Serrano, V.; Alexandre-Franco, M.; Lozano-Castelló, D.; Cazorla-Amorós, D.; Domingo-García, M., Effect of the surface chemical groups of activated carbons on their surface adsorptivity to aromatic adsorbates based on π-π interactions. *Mater. Chem. Phys.* **2014,** *143* (3), 1489-1499.

66. Göckeler, M.; Berger, C. M.; Purcel, M.; Bergsträßer, R.; Schinkel, A.-P.; Muhler, M., Surface reactions during temperature-programmed desorption and reduction experiments with oxygen-functionalized carbon blacks. *Appl. Surf. Sci.* **2021,** *561*, 150044.

67. Zhou, J.-H.; Sui, Z.-J.; Zhu, J.; Li, P.; Chen, D.; Dai, Y.-C.; Yuan, W.-K., Characterization of surface oxygen complexes on carbon nanofibers by TPD, XPS and FT-IR. *Carbon* **2007,** *45* (4), 785-796.

68. Li, N.; Ma, X.; Zha, Q.; Kim, K.; Chen, Y.; Song, C., Maximizing the number of oxygen-containing functional groups on activated carbon by using ammonium persulfate and improving the temperature-programmed desorption characterization of carbon surface chemistry. *Carbon* **2011,** *49* (15), 5002-5013.

69. Vivo-Vilches, J. F.; Bailón-García, E.; Pérez-Cadenas, A. F.; Carrasco-Marín, F.; Maldonado-Hódar, F. J., Tailoring the surface chemistry and porosity of activated carbons:

Evidence of reorganization and mobility of oxygenated surface groups. *Carbon* **2014,** *68*, 520-530.

70. Marchon, B.; Carrazza, J.; Heinemann, H.; Somorjai, G. A., TPD and XPS studies of O_2, CO_2, and H_2O adsorption on clean polycrystalline graphite. *Carbon* **1988,** *26* (4), 507-514.

71. Shinde, V. M.; Skupien, E.; Makkee, M., Synthesis of highly dispersed Pd nanoparticles supported on multi-walled carbon nanotubes and their excellent catalytic performance for oxidation of benzyl alcohol. *Catal. Sci. Technol.* **2015,** *5* (8), 4144-4153.

72. Petek, U.; Ruiz-Zepeda, F.; Bele, M.; Gaberšček, M., Nanoparticles and Single Atoms in Commercial Carbon-Supported Platinum-Group Metal Catalysts. *Catalysts* **2019,** *9* (2), 134.

73. Rao, R. G.; Blume, R.; Hansen, T. W.; Fuentes, E.; Dreyer, K.; Moldovan, S.; Ersen, O.; Hibbitts, D. D.; Chabal, Y. J.; Schlögl, R.; Tessonnier, J.-P., Interfacial charge distributions in carbon-supported palladium catalysts. *Nat. Commun.* **2017,** *8* (1), 340.

74. Rivera-Cárcamo, C.; Gerber, I. C.; del Rosal, I.; Guicheret, B.; Castro Contreras, R.; Vanoye, L.; Favre-Réguillon, A.; Machado, B. F.; Audevard, J.; de Bellefon, C.; Philippe, R.; Serp, P., Control of the single atom/nanoparticle ratio in Pd/C catalysts to optimize the cooperative hydrogenation of alkenes. *Catal. Sci. Technol.* **2021,** *11* (3), 984-999.

75. Wang, C.; Guan, E.; Wang, L.; Chu, X.; Wu, Z.; Zhang, J.; Yang, Z.; Jiang, Y.; Zhang, L.; Meng, X.; Gates, B. C.; Xiao, F.-S., Product Selectivity Controlled by Nanoporous Environments in Zeolite Crystals Enveloping Rhodium Nanoparticle Catalysts for CO_2 Hydrogenation. *J. Am. Chem. Soc.* **2019,** *141* (21), 8482-8488.

76. Khoobiar, S., Particle to Particle Migration of Hydrogen Atoms on Platinum—Alumina Catalysts from Particle to Neighboring Particles. *J. Phys. Chem.* **1964,** *68* (2), 411-412.

77. Vanoye, L.; Guicheret, B.; Rivera-Cárcamo, C.; Audevard, J.; Navarro-Ruiz, J.; del Rosal, I.; Gerber, I. C.; Campos, C. H.; Machado, B. F.; Volkman, J.; Philippe, R.; Serp, P.; Favre-Réguillon, A., Deactivation of Pd/C catalysts by irreversible loss of hydrogen spillover ability of the carbon support. *J. Catal.* **2023,** *424*, 173-188.

78. Wang, Y.; He, Q.; Guo, J.; Wei, H.; Ding, K.; Lin, H.; Bhana, S.; Huang, X.; Luo, Z.; Shen, T. D.; Wei, S.; Guo, Z., Carboxyl Multiwalled Carbon-Nanotube-Stabilized Palladium Nanocatalysts toward Improved Methanol Oxidation Reaction. *ChemElectroChem* **2015,** *2* (4), 559-570.

79. Machado, B. F.; Oubenali, M.; Rosa Axet, M.; Trang Nguyen, T.; Tunckol, M.; Girleanu, M.; Ersen, O.; Gerber, I. C.; Serp, P., Understanding the surface chemistry of carbon nanotubes: Toward a rational design of Ru nanocatalysts. *J. Catal.* **2014,** *309*, 185-198.

80. Zheng, Z.; Chen, M.; Zheng, X.; Liu, K.; Yang, T.; Zhang, J., Hydrogen Spillover Facilitating Reduction of Surface Oxygen Species on Porous Carbon. *ChemistrySelect* **2021,** *6* (9), 2178-2183.

81. Bhowmick, R.; Rajasekaran, S.; Friebel, D.; Beasley, C.; Jiao, L.; Ogasawara, H.; Dai, H.; Clemens, B.; Nilsson, A., Hydrogen Spillover in Pt-Single-Walled Carbon Nanotube Composites: Formation of Stable C−H Bonds. *J. Am. Chem. Soc.* **2011,** *133* (14), 5580-5586.

82. Montes-Morán, M. A.; Suárez, D.; Menéndez, J. A.; Fuente, E., On the nature of basic sites on carbon surfaces: an overview. *Carbon* **2004,** *42* (7), 1219-1225.

83. Menéndez, J. A.; Radovic, L. R.; Xia, B.; Phillips, J., Low-Temperature Generation of Basic Carbon Surfaces by Hydrogen Spillover. *J. Phys. Chem.* **1996,** *100* (43), 17243-17248.

84. Berlowitz, P. J.; Goodman, D. W., Chemisorption of ultrathin palladium layers on tungsten(110) and tungsten(100): adsorption of hydrogen and carbon monoxide. *Langmuir* **1988,** *4* (5), 1091-1095.

85. de la Puente, G.; Pis, J. J.; Menéndez, J. A.; Grange, P., Thermal stability of oxygenated functions in activated carbons. *J. Anal. Appl. Pyrolysis* **1997,** *43* (2), 125-138.

86. Udomsap, P.; Meesiri, S.; Chollacoop, N.; Eiad-Ua, A., Biomass Nanoporous Carbon-Supported Pd Catalysts for Partial Hydrogenation of Biodiesel: Effects of Surface Chemistry on Pd Particle Size and Catalytic Performance. *Nanomater.* **2021,** *11* (6), 1431.

87. Kwan, Y. C. G.; Ng, G. M.; Huan, C. H. A., Identification of functional groups and determination of carboxyl formation temperature in graphene oxide using the XPS O 1s spectrum. *Thin Solid Films* **2015,** *590*, 40-48.

88. Kundu, S.; Wang, Y.; Xia, W.; Muhler, M., Thermal Stability and Reducibility of Oxygen-Containing Functional Groups on Multiwalled Carbon Nanotube Surfaces: A Quantitative High-Resolution XPS and TPD/TPR Study. *J. Phys. Chem. C* **2008,** *112* (43), 16869-16878.

89. Herold, F.; Gläsel, J.; Etzold, B. J. M.; Rønning, M., Can Temperature-Programmed Techniques Provide the Gold Standard for Carbon Surface Characterization? *Chem. Mater.* **2022,** *34* (19), 8490-8516.

90. Campos-Delgado, J.; Kim, Y. A.; Hayashi, T.; Morelos-Gómez, A.; Hofmann, M.; Muramatsu, H.; Endo, M.; Terrones, H.; Shull, R. D.; Dresselhaus, M. S.; Terrones, M., Thermal stability studies of CVD-grown graphene nanoribbons: Defect annealing and loop formation. *Chem. Phys. Lett.* **2009,** *469* (1), 177-182.

91. Rivera-Cárcamo, C.; Scarfiello, C.; García, A. B.; Tison, Y.; Martinez, H.; Baaziz, W.; Ersen, O.; Le Berre, C.; Serp, P., Stabilization of Metal Single Atoms on Carbon and TiO_2

Supports for CO2 Hydrogenation: The Importance of Regulating Charge Transfer. *Adv. Mater. Interfaces* **2021,** *8* (8), 2001777.

92. Ghogia, A. C.; Machado, B. F.; Cayez, S.; Nzihou, A.; Serp, P.; Soulantica, K.; Pham Minh, D., Beyond confinement effects in Fischer-Tropsch Co/CNT catalysts. *J. Catal.* **2021,** *397*, 156-171.

93. Chou, P.; Vannice, M. A., Calorimetric heat of adsorption measurements on palladium: I. Influence of crystallite size and support on hydrogen adsorption. *J. Catal.* **1987,** *104* (1), 1-16.

94. Liu, W.; Magnin, Y.; Förster, D.; Bourgon, J.; Len, T.; Morfin, F.; Piccolo, L.; Amara, H.; Zlotea, C., Size-dependent hydrogen trapping in palladium nanoparticles. *J. Mater. Chem. A* **2021,** *9* (16), 10354-10363.

95. Ferrante, F.; Prestianni, A.; Bertini, M.; Duca, D., H_2 Transformations on Graphene Supported Palladium Cluster: DFT-MD Simulations and NEB Calculations. *Catalysts* **2020,** *10* (11), 1306.

96. Han, S. S.; Kim, H.; Park, N., Effect of Shuttling Catalyst on the Migration of Hydrogen Adatoms: A Strategy for the Facile Hydrogenation of Graphene. *J. Phys. Chem. C* **2011,** *115* (50), 24696-24701.

97. Zhao, Y.; Gennett, T., Water-Mediated Cooperative Migration of Chemisorbed Hydrogen on Graphene. *Phys. Rev. Lett.* **2014,** *112* (7), 076101.

98. Ramos-Castillo, C. M.; Reveles, J. U.; Zope, R. R.; de Coss, R., Palladium Clusters Supported on Graphene Monovacancies for Hydrogen Storage. *J. Phys. Chem. C* **2015,** *119* (15), 8402-8409.

99. Singh, A. K.; Ribas, M. A.; Yakobson, B. I., H-Spillover through the Catalyst Saturation: An Ab Initio Thermodynamics Study. *ACS Nano* **2009,** *3* (7), 1657-1662.

100. Gerber, I. C.; Serp, P., A Theory/Experience Description of Support Effects in Carbon-Supported Catalysts. *Chem. Rev.* **2020,** *120* (2), 1250-1349.

101. Kefalidis, C. E.; Perrin, L.; Burns, C. J.; Berg, D. J.; Maron, L.; Andersen, R. A., Can a pentamethylcyclopentadienyl ligand act as a proton-relay in f-element chemistry? Insights from a joint experimental/theoretical study. *Dalton Trans.* **2015,** *44* (6), 2575-2587.

102. Reiners, M.; Baabe, D.; Münster, K.; Zaretzke, M.-K.; Freytag, M.; Jones, P. G.; Coppel, Y.; Bontemps, S.; Rosal, I. d.; Maron, L.; Walter, M. D., NH_3 formation from N_2 and H_2 mediated by molecular tri-iron complexes. *Nat. Chem.* **2020,** *12* (8), 740-746.

103. Zhou, J.; Yang, P.; Kots, P. A.; Cohen, M.; Chen, Y.; Quinn, C. M.; de Mello, M. D.; Anibal Boscoboinik, J.; Shaw, W. J.; Caratzoulas, S.; Zheng, W.; Vlachos, D. G., Tuning the

reactivity of carbon surfaces with oxygen-containing functional groups. *Nat. Commun.* **2023,** *14* (1), 2293.

104. Chen, L.; Cooper, A. C.; Pez, G. P.; Cheng, H., Mechanistic Study on Hydrogen Spillover onto Graphitic Carbon Materials. *J. Phys. Chem. C* **2007,** *111* (51), 18995-19000.

105. Audevard, J.; Navarro-Ruiz, J.; Bernardin, V.; Tison, Y.; Corrias, A.; Del Rosal, I.; Favre-Réguillon, A.; Philippe, R.; Gerber, I. C.; Serp, P., Adjustment of the Single Atom/Nanoparticle Ratio in Pd/CNT Catalysts for Phenylacetylene Selective Hydrogenation. *ChemCatChem* **2023,** *15* (11), e202300036.

106. Chandrachud, P.; Pujari, B. S.; Haldar, S.; Sanyal, B.; Kanhere, D. G., A systematic study of electronic structure from graphene to graphane. *J. Condens. Matter Phys.* **2010,** *22* (46), 465502.

107. Lu, Y.; Huang, L.; Guo, Y.; Yang, X., Theoretical insights into origin of graphene oxide acidity and relating behavior of oxygen-containing groups in water. *Carbon* **2021,** *183*, 355-361.

108. Fan, G.; Huang, W.; Wang, C., In situ synthesis of Ru/rGO nanocomposites as a highly efficient catalyst for selective hydrogenation of halonitroaromatics. *Nanoscale* **2013,** *5* (15), 6819-6825.

109. Zhang, M.; Sun, Y.; Han, X.; Guo, W.; Cheng, Z.; Zou, Y.; Zhang, S., Modifying Interface of Carbon Support-Stimulated Hydrogen Spillover for Selective Hydrogenation. *J. Phys. Chem. C* **2022,** *126* (39), 16682-16689.

110. Mahdavi-Shakib, A.; Whittaker, T. N.; Yun, T. Y.; Sravan Kumar, K. B.; Rich, L. C.; Wang, S.; Rioux, R. M.; Grabow, L. C.; Chandler, B. D., The role of surface hydroxyls in the entropy-driven adsorption and spillover of H_2 on Au/TiO_2 catalysts. *Nat. Catal.* **2023,** *6* (8), 710-719.

111. Xing, S.; Xiong, M.; Zhao, S.; Zhang, B.; Qin, Y.; Gao, Z., Improving the Efficiency of Hydrogen Spillover by an Organic Molecular Decoration Strategy for Enhanced Catalytic Hydrogenation Performance. *ACS Catal.* **2023,** *13* (6), 4003-4011.